# Stability Analysis of Legged Locomotion Models by Symmetry-Factored Return Maps

Richard Altendorfer, Daniel E. Koditschek
Dept. of Electrical Engineering and Computer Science,
The University of Michigan, Ann Arbor, MI 48109, USA

Philip Holmes
Dept. of Mechanical and Aerospace Engineering,
Princeton University, Princeton, NJ 08544, USA

September 8, 2003

## Abstract

We present a new stability analysis for hybrid legged locomotion systems based on the "symmetric" factorization of return maps. We apply this analysis to 2 and 3 degree of freedom (DOF) models of the Spring Loaded Inverted Pendulum (SLIP) with different leg recirculation strategies. Despite the non-integrability of the SLIP dynamics, we obtain a necessary condition for asymptotic stability (and a sufficient condition for instability) at a fixed point, formulated as an exact algebraic expression in the physical parameters. We use this expression to study a variety of 2 DOF SLIP models that have previously been posited as low dimensional representations of running, focusing on the sensory "cost" required to achieve "fast" transients as measured by the degree of singularity of the linearized dynamics. We introduce a new 3 DOF SLIP model with pitching dynamics whose stability properties, revealed by this analysis, provide for the first time the beginnings of a formal explanation for the surprisingly stable gaits of the open loop controlled robot, RHex.

Keywords – legged locomotion, hybrid system, return map, Spring Loaded Inverted Pendulum, stability, time-reversal symmetry

## 1 Introduction

This paper introduces a new formalism for studying the stability of legged locomotion gaits and other periodic dynamically dexterous robotic tasks. We are motivated in part by the need to explain and control the remarkable performance of RHex, an autonomous hexapedal running machine whose introduction broke all prior published records for speed, specific resistance, and mobility over broken terrain [1]. Powered by only six actuators, located at the "hips" to drive each of its six passively compliant legs, in the manner of single-spoked rimless wheels, RHex's locomotion is excited by a single periodic "clock" signal split into phase and anti-phase copies for coordinating its alternating tripod gait. A simple PD controller at each hip motor in a given tripod forces its leg to track the alternately fast and slow clock reference signal corresponding to presumed stance and swing phases. Experimentally, RHex's performance at various speeds over various terrains is strongly dependent upon the particular values of the clock parameters, and, as is typical within the feedforward control paradigm, each new situation demands its own carefully tuned parameter set. Better analytical understanding of the relationship between clock signal and steady state gait should dramatically simplify the frequently lengthy empirical parameter tuning exercises presently required to achieve high performance gaits.

### 1.1 The SLIP Model as a Template for RHex

A complete account of the relationship between RHex's clock signal and steady state gait in even the simplest case would entail insight into the steady state properties of an under-actuated high degree of freedom (DOF) hybrid mechanical system whose Lagrangian dynamics switches among a set of $2^6$ possible holonomically constrained models depending upon which feet are in contact with the ground. Fortunately, a growing body of simulation study and empirical evidence [2] suggests that RHex, when properly tuned,

# Report Documentation Page

*Form Approved*
*OMB No. 0704-0188*



| 1. REPORT DATE | 2. REPORT TYPE | 3. DATES COVERED |
|---|---|---|
| **2003** | | **00-00-2003 to 00-00-2003** |

| 4. TITLE AND SUBTITLE | 5a. CONTRACT NUMBER |
|---|---|
| **Stability Analysis of Legged Locomotion Models by Symmetry-Factored Return Maps** | 5b. GRANT NUMBER |
| | 5c. PROGRAM ELEMENT NUMBER |
| 6. AUTHOR(S) | 5d. PROJECT NUMBER |
| | 5e. TASK NUMBER |
| | 5f. WORK UNIT NUMBER |
| 7. PERFORMING ORGANIZATION NAME(S) AND ADDRESS(ES) **University of Michigan,Computer Science and Engineering Division,Department of Electrical Engineering and Computer Science,Ann Arbor,MI,48109-2122** | 8. PERFORMING ORGANIZATION REPORT NUMBER |
| 9. SPONSORING/MONITORING AGENCY NAME(S) AND ADDRESS(ES) | 10. SPONSOR/MONITOR'S ACRONYM(S) |
| | 11. SPONSOR/MONITOR'S REPORT NUMBER(S) |

12. DISTRIBUTION/AVAILABILITY STATEMENT
**Approved for public release; distribution unlimited**

13. SUPPLEMENTARY NOTES
**The original document contains color images.**

14. ABSTRACT

15. SUBJECT TERMS

| 16. SECURITY CLASSIFICATION OF: | | | 17. LIMITATION OF ABSTRACT | 18. NUMBER OF PAGES | 19a. NAME OF RESPONSIBLE PERSON |
|---|---|---|---|---|---|
| a. REPORT **unclassified** | b. ABSTRACT **unclassified** | c. THIS PAGE **unclassified** | | **28** | |

exhibits sagittal plane stance behavior well approximated by the two degree of freedom SLIP. This comes in addition to the well-established fact that the centers of mass of running animals [3] and humans [4] approximately follow the dynamics of the sagittal plane SLIP. A general framework for "anchoring" the SLIP-"template" mechanics in the far more elaborate morphologies of real animals' bodies has been introduced in [5]. Briefly, given a high-dimensional dynamical system – the "anchor" – that is believed to be a reasonably accurate model of an animal or robot, a "template" is a low-dimensional dynamical system whose steady state encodes the task and is conjugate to the restriction dynamics of the anchor on an attracting invariant submanifold.

In general, both the anchoring as well as the control of the SLIP template seem to demand sensing, actuation, and computation that may be unrealistic relative to the resources that animals and practical robots might possess. Indeed, a hierarchical controller [6] for a RHex-like simulation model programmed in SimSect [7] that enforces both the anchoring as well as the template control relies on sophisticated full state feedback. A part of the sensor-suite necessary to implement this feedback control has only recently been installed on the robot [8] and it is currently unknown whether the stabilizing effect of this controller seen in simulation will persist in the presence of unavoidable sensor noise. This motivates the question: is it possible to implement the template-anchor paradigm [5] with sensor-cheap, low-bandwidth robotic controllers?

In this paper we address that part of the above question concerned with template control. Namely given that a SLIP-anchoring mechanism is present, either by deliberate design or by the interaction of the controlled robot with its environment, can the stability and performance of the controlled template be assessed methodically (beyond empirical or numerical study), for example, as a function of the cost of the sensory feedback required?

## 1.2 Output feedback stabilization in the SLIP model

The SLIP model is a hybrid dynamical system formed by the composition of leg-body stance dynamics with ballistic body flight dynamics. Control takes place during the flight phase, where the leg angle is set for the next touchdown event. The two degree of freedom SLIP model provides a ubiquitous description of biological runners in the sagittal plane [3] and, as mentioned above, a broadly useful prescription for legged robot runners such as RHex [9, 1, 2] as well. The closely related three degree of freedom Lateral Leg Spring (LLS) model, has been recently identified as a candidate template for cockroach running in the horizontal plane [10, 11] and seems likely to be relevant for RHex as well [1].

However, the limitations of the two degree of freedom SLIP model (no pitching dynamics, no lateral dynamics) and the three degree of freedom LLS model (failure to reproduce some aspects of animal data [12]) show that far more sophisticated models will be required to capture more salient features of the anchor. In particular, a literal template of RHex, i. e. a model whose dynamics represents the restriction dynamics of an attracting invariant submanifold in RHex, must include a source of dissipation as well as hip torques. Despite these shortcomings, the two degree of freedom SLIP and its extension to three degrees of freedom (introduction of pitch dynamics) are sufficiently well motivated by prior literature, sufficiently mathematically challenging (due to their non-integrable nature) and their analysis sufficiently revealing of RHex-like properties (as is shown below) as to motivate our exclusive focus on them in this paper.

The stability properties of these hybrid dynamical systems can be assessed by a Poincaré or return map $R$ acting on a (reduced) Poincaré section $\mathcal{X}$:

$$R : \mathcal{X} \to \mathcal{X} \ . \tag{1}$$

In legged locomotion, the iterates of this return map $R$ – the function relating the body state at a periodically (at each stride) occurring event – summarizes all properties relevant to the goal of translating the body center of mass. The return map arises in general from a controlled plant model

$$\begin{aligned} x(k+1) &= A(x(k), u(k)) \\ y(k) &= C(x(k)) \end{aligned} \tag{2}$$

where the discrete time control input variable, $u(k)$, represents the consequences at the integrated stride-by-stride level of controlled influences imposed over continuous time within stance or flight. In this paper, physically motivated assumptions (listed in Section 2.4.1) that we impose upon the allowable continuous time influences turn out to yield a discrete time representative, $u$, that implicitly determines the flight time for the ballistic phase of the body at each stride. When the continuous time physical influences imposed within a given stride are determined according to state information gathered from the available observations of the previous stride, we have effectively introduced a discrete time feedback policy,

$$u(k) = H(y(k)) \tag{3}$$

whose closed loop yields (1), $R(x) = A(x, H \circ C(x))$. The controlled plant model for SLIP systems is specified in Section 2.4.3.

In this paper we will confine our study exclusively to such time invariant output feedback laws, $H$ (3) for two allied reasons. First, this restriction focuses attention on the key role played by the output function, $C$ (2), variations of which we will use to model sensor limitations of the underlying physical system represented by the SLIP model. Second, since $u$ models the influence of flight phase duration (implicitly by specifying the leg angle trajectory), this restriction to time invariant output feedback, $H$ (3), models the leg recirculation policies that have so rightly captured the attention of the legged locomotion community in recent years.

The surprising discovery of "self-stable" legged locomotion – first in the closely related LLS model [11]; subsequently in the SLIP itself [13, 14] – demands a more systematic account of what is meant by the term "self." In these studies, the duration of flight phase is determined by a fixed leg angle policy, and "self" connotes the apparent absence of active sensors. Recently, a more elaborate state-dependent leg retraction policy has been shown numerically to inherit the stability properties of the fixed touchdown angle policy while increasing the basin of the stable gait [15]. On the other hand, a recirculation policy that initiates after leg liftoff a constant angular velocity until leg touchdown can induce neutral stability [16]. These apparently slightly varied policies mask significant variation in cost and effort depending upon how the sensor suite might be implemented in practice. We seek to shed greater light on when a more or less clever leg recirculation strategy can make a difference in the quality of gait stability (e.g., faster transients, larger basin) as a function of the "cost" of sensory data.

Of course, real sensors are not implemented in these templates at all but in physical machines. Empirically, it is abundantly clear that the leg swing policy plays a central role in the gait quality of physically useful machines such as RHex [1]. Leg recirculation strategies have been shown numerically to play a key role in the gait quality of independent locomotion models inspired by quadrupedal animal trotters [17] and gallopers [18]. When the SLIP template is anchored actively [6] then its stability properties determine those of the anchor by definition, hence insight into how to tune the quality of SLIP gaits transfers directly over to the physical machine of interest. However, in the absence of complete state feedback, the correspondence between the template and the behavior of a complex system that shows empirical evidence of anchoring it is not at all clear.

Lacking formal results bearing on this issue, we find it useful to introduce terminology summarizing the following intuitive distinction. We will say that the correspondence is "descriptive" if properties observed in the complex model are also observed in the template model fitted to it. We will say that the correspondence is "prescriptive" if design parameter settings in the complex model indeed anchor and yield as well the same properties they produce in the template model.

## 1.3 Contribution of this paper

Notwithstanding its apparent simplicity, the SLIP model is non-integrable: the stance phase trajectory cannot be written down in closed form [19]. This has motivated authors who seek insight more systematic than numerical simulation can provide to develop various physically motivated closed form approximations to $R$ instead [20, 21, 22]. In contrast, here we observe that while $R$ cannot be written in closed form, certain physically reasonable assumptions (listed in Section 2.4.1, below) imply that the determinant of its Jacobian at a *symmetric* fixed point (to be defined in Section 2.3) of $R$ can be so expressed. The central contributions of this paper arising from that observation include:

1. A new analytical framework based on a "symmetric" factorization of the return map $R$, in terms of its non-hybrid components that yields the closed form expression of the determinant at a symmetric fixed point of $R$ (Section 3). Necessary conditions for asymptotic stability, sufficient conditions for instability, and conditions equivalent to neutral stability of the closed loop map, $R$, follow.

2. Closed form conditions on $H \circ C$ yielding rigorous statements concerning the sensory "cost" of control in both the 2 DOF and 3 DOF settings that cannot be established by mere numerical study, as follows:

   (a) 2 DOF SLIP models: any control with fast transients ("singular" control: the Jacobian of the closed loop return map is globally singular) requires velocity sensing and is therefore "costly" (Section 3.3.1).

   (b) 3 DOF SLIP models: SLIP models that have only non-inertial (body frame) sensors available cannot implement singular control (Section 3.4.1).

3. A new 3 DOF SLIP model based upon the RHex gait generator [1] which, when subject to the

factored stability analysis, imposes for the first time analytical conditions on RHex's "feedforward clock" parameters [1] necessary for the stability (and sufficient for instability) of the resulting 3 DOF gait (Section 3.4.2).

4. A preliminary numerical study in Section 4 suggesting that our 3 DOF SLIP model is a good descriptive model of a RHex-like 24 DOF model (programmed in SimSect [7]).

In Section 2 we preface this analysis by introducing the terminology and notation for hybrid systems to be used subsequently, followed by a review of how reversibility symmetries can replace the symplectic symmetry in Liouville's theorem (see e.g. [23]), which does not generally apply to hybrid systems. We then develop the consequences of these observations in Section 3 along the lines described above, present a preliminary numerical study in Section 4, and close with some brief concluding remarks in Section 5.

# 2 Theoretical framework and modeling assumptions

In section 2.1 we introduce the terminology of hybrid dynamical systems and provide some intuition concerning the machinery used to trim away the awkward and inessential details of our hybrid model to yield a conventional discrete dynamical control system (2) whose closed loop properties (1) represent the formal object of study. Having established a notation for (hybrid) dynamical systems, Liouville's theorem, a key tool in the present study, can be stated formally in the next section, 2.2. Then an analogue of the local form of Liouville's theorem for discrete maps derived from hybrid systems will be established in Section 2.3. Section 2.4 formally defines the SLIP system with its hybrid components as well as its Poincaré section and discrete time return map.

## 2.1 Preliminary definitions and modeling considerations of hybrid dynamical systems

Models of legged locomotion are characterized by distinct phases, notably, stance and flight. Formally, the dynamics cannot be described by a single flow, but require a collection of continuous flows and discrete transformations governing their transitions. The resulting model is called a "hybrid" system. This section makes the notion of a hybrid system more precise by adapting the definitions in [24] to the present setting.

Let $\mathcal{I}$ be a finite index set and $\mathcal{X}_\alpha, \alpha \in \mathcal{I}$ with $\dim(\mathcal{X}_\alpha) = 2N$ a collection of open Euclidean domains (charts). Assume a mechanical system whose time evolution is described by holonomically constrained autonomous conservative vector fields $f_\alpha$, with configuration space variables $q$: $\dot{x} = f_\alpha(x)$ with $x = (q\ \dot{q})^\top \in \mathcal{X}_\alpha$. Transitions from one vector field $f_\alpha$ to another vector field $f_\beta$ are governed by threshold functions $h_\alpha^\beta$ which specify an event at their zero-crossing. The threshold functions $h_\alpha^\beta$ can depend on the initial condition $x_0 = x(t=0) \in \mathcal{X}_\alpha$, time $t$, and the current state $f_\alpha^t(x_0) =: x(t)$.[1] We restrict ourselves to hybrid systems where for each chart there is only one threshold function $h_\alpha^\beta$; hence the upper index $\beta$ will be dropped from now on. We also reset the time to zero at each chart transition. The end time of the evolution on chart $\mathcal{X}_\alpha$ is uniquely defined by $t_\alpha(x_0) = \min_{t>0}\{t : h_\alpha(f_\alpha^t(x_0), x_0, t) = 0\}$. The equation $h_\alpha(f_\alpha^t(x_0), x_0, t) = 0$ will be referred to as the threshold equation. Switching between charts is effected by transition mappings $T_\alpha^\beta$ with domains in $\mathcal{X}_\alpha$ and ranges in $\mathcal{X}_\beta$. The *flow map* $F_\alpha$ for the $\alpha$th vectorfield is defined via the implicit function, $t_\alpha$, $F_\alpha : x_0 \mapsto f_\alpha^{t_\alpha(x_0)}(x_0)$.[2]

In this paper, as in many settings of hybrid dynamical systems, we are interested in the attractive behavior of distinguished orbits whose appropriate projections are periodic. By "periodic" we mean that the distinguished orbit is defined on a recurring sequence of charts along which the projected flow yields a return to the same projected initial condition. An "appropriate" projection strips away variables whose values are not descriptive of the locomotion task – here, the conserved total mechanical energy along with the cyclic variable of elapsed distance. Similarly, "attractive behavior" denotes the asymptotic properties of projected orbits relative to the projection of the distinguished orbit. These slight variants of the traditional Poincaré analysis of conventional dynamical systems theory will all be introduced formally in the next section, and will be seen to yield a *stride* map

$$S = S_2 \circ S_1 \tag{4}$$

whose projection (along with those of its factors, $S_\alpha$) that we will denote $R$ (along with the corresponding factors, $R_\alpha$) captures as a discrete time iterated dynamical system the locomotion relevant behavior of

[1] Note that this is more general than the definition in [24], where $h_\alpha^\beta$ only depends on $f_\alpha^t(x_0)$. This added generality is required because we wish to study the effects of leg recirculation strategies – reference trajectories parametrized by time that are triggered by a liftoff transition - see e.g. equation (47).

[2] Note that $F_\alpha$ is not the usual constant-time flow map of dynamical systems theory $f_\alpha^t(x_0)$; rather the time varies depending upon the initial data $x_0$.

our hybrid dynamical system analogous to a Poincaré map.

## 2.2 Liouville's theorem and stability

Informally, Liouville's theorem states that volume in phase space of a holonomically constrained conservative dynamical system described by a single Hamiltonian flow is preserved, i.e. a set of initial conditions at $t = 0$ in phase space will be mapped to a set with identical symplectic volume for any $t \geq 0$. More formally, Liouville's theorem appears in two equivalent formulations, the local and the global form [23].

**Theorem 1 (Liouville's theorem (local form))** *Let $f^t(x)$ be the flow of a vector field $f$ on a chart $\mathcal{X}$ of a Hamiltonian system, i.e. $\exists H : \mathcal{X} \to \mathbb{R}$ with $\dim(\mathcal{X}) = 2N, N \in \mathbb{N}$ such that*

$$f(x) = \begin{pmatrix} 0 & \mathbf{1}_{N\times N} \\ -\mathbf{1}_{N\times N} & 0 \end{pmatrix} D_x H(x) \quad \forall x \in \mathcal{X} \qquad (5)$$

*Then for all $x \in \mathcal{X}$ and for all times $t$ for which the flow is defined,*

$$D_x f^t(x) \in \mathrm{Sp}_{2N}; \quad \det\left(D_x f^t(x)\right) = 1 \qquad (6)$$

*($\mathrm{Sp}_{2N}$ denotes the group of symplectic matrices of size $2N\times 2N$.) The matrix of partial derivatives of the flow with respect to the initial conditions $x$ is symplectic and its determinant is one.*

The global form states that $f^t$ maps a measurable set of initial conditions to a set of equal measure.

**Definition 1 (Volume preservation)** *A map $S : \mathcal{X} \to \mathcal{X}$ is locally volume preserving at a point $x \in \mathcal{X}$ if $|\det(D_x S(x))| = 1$. Its local volume at $x$ is defined to be $\det(D_x S(x))$. It is volume preserving (or globally volume preserving) if $|\det(D_x S(x))| = 1\ \forall x \in \mathcal{X}$.*

This definition retains the familiar informal notion of volume preservation (the "global" integral version arises, after all, from the local determinant condition) at the expense of a slight degree of imprecision in terminology. Upon cursory inspection, it might be thought that conservative "piecewise holonomic" [25] systems automatically satisfy the hypotheses of Liouville's theorem. By fixing $t$ at a particular but arbitrary time $\bar{t}$, a "degenerate" hybrid dynamical system can be defined on a single chart $\mathcal{X}_1 = \mathcal{X}$ with one vectorfield $f_1 = f$ and the threshold function $h_1(f^t(x_0), x_0, t) = t - \bar{t}$. The resulting stride map $S = F_1 = f^{t_1}(\cdot)$ with $t_1 = \bar{t}$ then obviously satisfies $\det(D_x S(x)) = 1 \quad \forall x \in \mathcal{X}$. However, for a threshold equation that is not purely time-dependent but also depends on $f^t(x_0)$ and $x_0$, the evolution time $t_1$ is dependent upon the initial condition: $t_1 = t_1(x_0)$, and $\det\left(D_x f^{t_1(x_0)}(x_0)\right) \neq 1$ in general. Hence for a general hybrid dynamical system in which the threshold functions are not purely time-dependent, the determinant of the Jacobian of the stride map $S$ (4) cannot be expected to be of absolute value one, even if all the vector fields are Hamiltonian and all transition functions are volume preserving.

Liouville's theorem precludes the asymptotic stability of a Hamiltonian system, since an asymptotically stable equilibrium point reduces a finite phase space volume to a single point. This would require $\lim_{t\to\infty} \det(D_x f^t(x)) = 0$ for all $x$ in the basin of attraction of the asymptotically stable equilibrium point. However, because Liouville's theorem is not guaranteed to apply, asymptotic stability of piecewise-defined holonomically constrained conservative Hamiltonian systems whose discrete time behavior can be described by an appropriate projection of a stride map $S$,[3] has been observed in the literature. Examples include a discrete version of the Chaplygin sleigh [25, 26] and low-dimensional models of legged locomotion in the horizontal and sagittal planes [11, 13, 14]. In all of those cases, some threshold functions are not solely time-dependent and the stride map is not volume preserving – a necessary condition for asymptotic stability. In particular, at an asymptotically stable fixed point $\bar{x}$, $|\det(D_x S(\bar{x}))| < 1$.

Having established the non-applicability of Liouville's theorem to general hybrid dynamical systems, we will present criteria in the next section under which, nevertheless, the volume preservation property, $|\det(D_x S(\bar{x}))| = 1$ does indeed hold. The result could be called a point Liouville theorem for stride map fixed points, because in distinction to the local form of Liouville's theorem, which holds for all points of symplectic phase space, our theorem only holds at fixed points, $\bar{x}$, of $S$.

## 2.3 A point Liouville theorem for hybrid dynamical systems

In order to prove that $|\det(D_x S(\bar{x}))| = 1$ at a fixed point of $S$, additional assumptions and an additional structure of the underlying vectorfields $f_\alpha$ is needed. In particular, we require that the vectorfields $f_\alpha$ possess a time reversal symmetry (for a survey of time reversal symmetries in dynamical systems see [27]; for an extensive review see [28]):

[3] The term "piecewise holonomic system" was introduced in [25].

**Definition 2 (Time reversal symmetry)** *A vector field $f$ on a chart $\mathcal{X}$ admits a time reversal symmetry $G : \mathcal{X} \to \mathcal{X}$ with $G$ an involution*[4] *($G \circ G = id$) if*

$$D_x G \cdot f = -f \circ G. \tag{7}$$

*or, equivalently, if*

$$G \circ f^t = f^{-t} \circ G \ . \tag{8}$$

We will next introduce a further property of the stride map factors, $S_\alpha$, of $S = S_2 \circ S_1$, namely that they can be written as *time reversed flow maps* $S_\alpha = G_\alpha \circ F_\alpha$ or $S_\alpha = F_\alpha \circ G_\alpha$. We restrict our investigation to a subset of fixed points of $S$, namely the ones that are also fixed points of the time reversed flow maps $S_\alpha$, Such fixed points we will call *symmetric* in analogy to certain fixed points of reversible diffeomorphisms (see definition 6 in Appendix C.1). Fixed points of this kind will be shown to lie on distinguished orbits termed *symmetric* [29]; Such orbits have been recognized in the prior legged locomotion literature as useful steady state target trajectories in the control of one-legged hoppers [9] and also serve as steady state target trajectories in this paper.

**Definition 3 (Symmetric orbit of a time reversible vector field)**
*The orbit of a vector field $f$ with time reversal symmetry $G$ is called symmetric if it is invariant under $G$ [29]. This definition of symmetric orbits coincides with the notion of neutral orbits introduced in [9] and formalized in [30].*

**Theorem 2** *Let $\bar{x}$ be a fixed point of $S_\alpha = G_\alpha \circ F_\alpha$, where $F_\alpha$ is the flow map of a vector field $f_\alpha$ with time reversal symmetry $G_\alpha$. Then $\bar{x}$ lies on a symmetric orbit of $f_\alpha$.*
Proof: If $\bar{x}$ is a fixed point of $S_\alpha$ then there exists a time $\bar{t}$ such that $G_\alpha \circ f_\alpha^{\bar{t}}(\bar{x}) = \bar{x}$. If $\bar{x}$ lies on a symmetric orbit then $\forall t \in [0, \bar{t}]\ \exists t' \in [0, \bar{t}] : f_\alpha^{t'}(\bar{x}) = G_\alpha \circ f_\alpha^t(\bar{x})$. Let $t' = \bar{t} - t$. Then $f_\alpha^{t'}(\bar{x}) = G_\alpha \circ f_\alpha^{t-\bar{t}} \circ G_\alpha(\bar{x}) = G_\alpha \circ f_\alpha^t(\bar{x})$.

Clearly, $S$ locally preserves volume at a symmetric fixed point $\bar{x}$ if its time reversed flow maps do. On the other hand, involutions are known to be volume preserving at their fixed points:

**Theorem 3** *The determinant of the Jacobian of an involution $G : \mathbb{R}^N \to \mathbb{R}^N$ at a fixed point $\bar{x}$ of $G$ is plus or minus one.*
Proof:

$$\begin{aligned} G \circ G &= id \\ D(G \circ G)(x) &= \mathbf{1}_{N\times N} \quad \forall x \in \mathbb{R}^N \\ DG(G(x)) \cdot DG(x) &= \mathbf{1}_{N\times N} \end{aligned} \tag{9}$$

Since $G(\bar{x}) = \bar{x}$, (9) implies that:

$$\begin{aligned} DG(\bar{x}) \cdot DG(\bar{x}) &= \mathbf{1}_{N\times N} \\ \Rightarrow \det{}^2(DG(\bar{x})) &= 1 \end{aligned} \tag{10}$$

Hence a criterion for $S_\alpha$ being an involution is needed.

**Lemma 1** *If $t_\alpha$ is $S_\alpha$ invariant, that is, $t_\alpha \circ S_\alpha = t_\alpha$ on a set $\mathcal{X}_{h_\alpha}$, then $S_\alpha \circ F_\alpha$ is an involution on $\mathcal{X}_{h_\alpha}$.*
Proof: Let $x_0 \in \mathcal{X}_{h_\alpha}$.

$$\begin{aligned} S_\alpha \circ S_\alpha(x_0) &= \\ G_\alpha \circ F_\alpha \circ G_\alpha \circ F_\alpha(x_0) &= \\ G_\alpha \circ f_\alpha^{t_\alpha(S_\alpha(x_0))} \circ G_\alpha \circ f_\alpha^{t_\alpha(x_0)}(x_0) &= \\ f_\alpha^{-t_\alpha(S_\alpha(x_0))} \circ f_\alpha^{t_\alpha(x_0)}(x_0) &= x_0 \ . \end{aligned} \tag{11}$$

A condition for the $S_\alpha$ invariance of $t_\alpha$ is now given, in turn, as follows.

**Lemma 2** *A necessary condition for the $S_\alpha$ invariance of $t_\alpha$ is $h_\alpha(G_\alpha(x_0), G_\alpha \circ f_\alpha^{t_\alpha(x_0)}(x_0), t_\alpha(x_0)) = 0$ $\forall x_0 \in \mathcal{X}_{h_\alpha}$.*
Proof: If $t_\alpha$ is $S_\alpha$-invariant then $t_\alpha(x_0)$ must solve the threshold equation for $S_\alpha(x_0)$:

$$\begin{aligned} &h_\alpha(f_\alpha^{t_\alpha(x_0)} \circ G_\alpha \circ f_\alpha^{t_\alpha(x_0)}(x_0), G_\alpha \circ f_\alpha^{t_\alpha(x_0)}(x_0), t_\alpha(x_0)) = \\ &h_\alpha(G_\alpha(x_0), G_\alpha \circ f_\alpha^{t_\alpha(x_0)}(x_0), t_\alpha(x_0)) = 0 \end{aligned} \tag{12}$$

Assuming that $t_\alpha(x_0)$ is also the <u>minimal</u> solution of the threshold equation for $S_\alpha(x_0)$, it follows that the condition of Lemma 2 is also sufficient, and one concludes that $t_\alpha$ is invariant under $S_\alpha$. Lemma 2 essentially checks that the threshold function $h_\alpha$ "preserves" the time reversal symmetry of $f_\alpha$.

Combining Lemmas 1 and 2 and Theorem 3 constitutes a point-wise Liouville theorem for discrete systems of the form $S = S_2 \circ S_1$ at symmetric fixed points. The generalization to a stride map composed of more than two time reversed flow maps $S_\alpha$ is straightforward. As a final observation that we will require below (in Appendix A), note that if Theorem 3 has been shown to hold for $S_\alpha = G_\alpha \circ F_\alpha$, it also holds for reverse time flow maps of the form $S_\alpha = F_\alpha \circ G_\alpha$:

**Lemma 3** *If $S_\alpha = G_\alpha \circ F_\alpha$ is an involution, then $S'_\alpha = F_\alpha \circ G_\alpha$ is an involution, too.*

[4] In this paper, we restrict ourselves to involutive time reversal symmetries, although a more general definition can be found in [27].

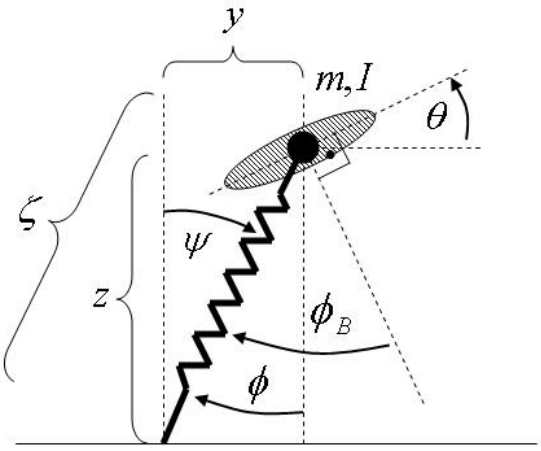


Figure 1: Coordinate convention of SLIP with pitching dynamics. In the text, the COM coordinates will be parametrized by cartesian coordinates, i. e. $y = \zeta \sin(\psi)$ and $z = \zeta \cos(\psi)$. In flight, the leg angle $\phi$ will in general be a function of time and of the SLIP's liftoff state: $\phi(t, x_0)$.

Proof:

$$\begin{aligned} {S'}_\alpha \circ {S'}_\alpha &= F_\alpha \circ G_\alpha \circ F_\alpha \circ G_\alpha \\ &= (G_\alpha \circ \underbrace{G_\alpha) \circ F_\alpha \circ G_\alpha \circ F_\alpha}_{=id} \circ G_\alpha \\ &= G_\alpha \circ G_\alpha = id \ . \end{aligned}$$

## 2.4 SLIP dynamics

### 2.4.1 Modeling assumptions

In this section we establish the specifics of the SLIP models considered in this paper. They are listed in terms of the categories: geometry, potential forces, control, and orbits:

**Geometry:** The 3 DOF sagittal plane SLIP model is shown in Fig. 1. It shows a rigid body of mass $\tilde{m}$ and moment of inertia $\tilde{I}$ with a massless springy leg with rest length $\tilde{\zeta}_0$ attached at a hip joint that coincides with the center of mass (COM). The strength of gravity is $\tilde{g}$. The approximation of a leg with zero mass avoids impact losses at touchdown and simplifies the control. For convenience, all of the following expressions are formulated in dimensionless quantities, i.e. $t = \tilde{t}\sqrt{\frac{\tilde{g}}{\tilde{\zeta}_0}}$, $y = \frac{\tilde{y}}{\tilde{\zeta}_0}$, $\dot{y} = \frac{\dot{\tilde{y}}}{\sqrt{\tilde{\zeta}_0 \tilde{g}}}$, $z = \frac{\tilde{z}}{\tilde{\zeta}_0}$, $\dot{z} = \frac{\dot{\tilde{z}}}{\sqrt{\tilde{\zeta}_0 \tilde{g}}}$, $\theta = \tilde{\theta}$, $\dot{\theta} = \dot{\tilde{\theta}}\sqrt{\frac{\tilde{\zeta}}{\tilde{g}}}$ and $I = \frac{\tilde{I}}{\tilde{m}\tilde{\zeta}_0^2}$. Also shown are the pitch angle $\theta$ with respect to the horizontal and the parametrization of the COM in terms of cartesian $(y, z)$ and polar $(\zeta = \sqrt{y^2 + z^2}, \psi = \arctan(y/z))$ coordinates with the coordinate origin at the foothold. The body is assumed to remain in the sagittal plane and its configuration is parametrized by $SE(2)$ coordinates $(y, z, \theta)$ or $(\zeta, \psi, \theta)$.

**Trajectories:** A full stride consists of a stance and a flight phase: in stance, we assume the foothold is fixed, the leg compressed and the body moves in the positive $y$ direction $\dot{y} > 0$; in flight, the body describes a ballistic trajectory under the sole influence of gravity. The stance phase starts with the leg uncompressed and ends when the leg has reached its rest length $\bar{\zeta}$ again. Then the flight phase begins and ends when the massless leg – appropriately placed – touches the ground. Stability investigations in this paper are confined to trajectories that are in the vicinity of symmetric trajectories in both stance and flight, where e.g. the liftoff and touchdown vertical heights are equal.

**Control:** No continuous control is exerted during stance and flight, the corresponding vector fields do not change from stride to stride. The only control authority consists in determining the transitions between flight and stance by specifying the stance and flight time. The stance time is implicitly determined by requiring the leg to undergo a compression-decompression cycle, hence the only designable control authority consists in specifying the flight time, which can be implicitly parametrized by the free leg angle trajectory $\phi(t, x_0)$ and hence touchdown COM height. Due to the massless assumption, the leg can be arbitrarily placed during flight at no energetic cost.

**Potential forces:**

**P1** The potential energy is given by $E_p = z + V(y, z, \theta)$.

**P2** The non-gravitational potential $V$ is analytic and satisfies the symmetry relation $V(y, z, \theta) = V(-y, z, -\theta)$. This condition does not seem to severely restrict our choice of potentials, and it includes the often-used radial spring potential $V(y, z, \theta) = V_r(\zeta)$ for the 2 DOF model.

**P3** $V$ factorizes as $V(y, z, \theta) = V_r(\zeta)V_p(y, z, \theta)$ with $V_r(1) = 0$. This ensures that $V$ is zero at touchdown and liftoff. Because of the masslessness of the leg, $V$ stays zero during flight.

After having listed SLIP's modeling assumptions, we will define the stance and flight components of the

hybrid SLIP system and identify time reversal symmetries present in its vectorfields.

### 2.4.2 Definition of the hybrid SLIP system

The SLIP system consists of two phases – stance and flight – hence $\mathcal{I} = \{1, 2\}$ with 1 referring to stance and 2 referring to flight. In both phases, we choose the same parametrization of the configuration space – by the cartesian coordinates of the mass center relative to the fixed toe, $y, z$, and the orientation in of the body in the inertial frame, $\theta$. Hence, both charts are equal, $\widehat{\mathcal{X}}_1 = \widehat{\mathcal{X}}_2 = R^2 \times \mathbb{S}^1 \times R^3 =: \widehat{\mathcal{X}}$ with phase space elements denoted by $\widehat{x} = (y, z, \theta, \dot{y}, \dot{z}, \dot{\theta})^\top$.

**Stance** The stance vector field reads

$$\widehat{f}_1(\widehat{x}) = \begin{pmatrix} \dot{y} \\ \dot{z} \\ \dot{\theta} \\ -\partial_y V(y, z, \theta) \\ -1 - \partial_z V(y, z, \theta) \\ -\frac{1}{I}\partial_\theta V(y, z, \theta) \end{pmatrix} \tag{13}$$

With **P2** this vector field is also analytic in $\widehat{x}$ and hence its flow $\widehat{f}_1^t(\widehat{x})$ is analytic in $t$ and $\widehat{x}$. Using **P3** $\widehat{f}_1$ admits the linear time reversal symmetry

$$\widehat{G}_1 = \mathrm{diag}(-1, 1, -1, 1, -1, 1) \ . \tag{14}$$

(the linear time reversal symmetry of (13) without pitching dynamics was already recognized in [30]). With the "radius" function $\zeta : \widehat{x} \mapsto \sqrt{y^2 + z^2}$, the threshold function is given by

$$h_1(\widehat{x}(t), \widehat{x}_0, t) = \zeta(\widehat{x}(t)) - \zeta(\widehat{x}_0) \tag{15}$$

**Flight** The flight vector field reads

$$\widehat{f}_2(\widehat{x}) = \Big(\dot{y}, \dot{z}, \dot{\theta}, 0, -1, 0\Big)^\top \tag{16}$$

whose analytic flow is trivially computed as

$$\widehat{f}_2^t(\widehat{x}_0) = \begin{pmatrix} y_0 + \dot{y}_0 t \\ z_0 + \dot{z}_0 t - \frac{t^2}{2} \\ \theta_0 + \dot{\theta}_0 t \\ \dot{y}_0 \\ \dot{z}_0 - t \\ \dot{\theta}_0 \end{pmatrix} \tag{17}$$

Solving eq. (7) with $\widehat{f}_2$, the diagonal linear involutive time reversing symmetry $\widehat{G}_2$ of (16) is not uniquely defined and is given by

$$\widehat{G}_2^{\mp} = \mathrm{diag}(\mp 1, 1, \mp 1, \pm 1, -1, \pm 1) \ . \tag{18}$$

As will become clear later in the next section, in order to define a stride map as in (4), the time reversal symmetries should match for stance and flight, hence $\widehat{G}_2^- = \widehat{G}_1 =: \widehat{G}$ is chosen.

The threshold function $h_2$ for a general leg placement parametrized by the angular trajectory $\phi(t, \widehat{x}_0)$ (see Fig. 1) becomes zero when the toe touches the ground

$$h_2(\widehat{x}(t), \widehat{x}_0, t) = z(t) - \cos(\phi(t, \widehat{x}_0)) \ . \tag{19}$$

and implicitly defines the control input $t_2(\widehat{x}_0)$. If $\phi$ depends on $\widehat{x}_0$ – the liftoff coordinates, feedback control is employed. The design of the function $\phi$ constitutes the control authority in our SLIP model.

### 2.4.3 Discrete time behavior of SLIP locomotion: Poincaré section, return map, and controlled plant model

**Poincaré section** A SLIP stride consists of stance and flight, therefore its stride map should be written as $\widehat{S} = \widehat{F}_2 \circ \widehat{F}_1$. The end of the stance phase is characterized by the liftoff event, detected by the threshold equation $h_1$; the end of flight is characterized by the touchdown event, detected by the threshold equation $h_2$. The factorization of $\widehat{S}$ suggests a Poincaré section $\mathcal{P}$ that is the surface of the touchdown event, where the leg length is one and the COM is to the left of the foothold:

$$\mathcal{P} = \{\widehat{x} \in \widehat{\mathcal{X}} : y^2 + z^2 - 1 = 0, y < 0\} \ . \tag{20}$$

**Return map** We would like to factor $\widehat{S}$ into time reversed flow maps $\widehat{S}_\alpha$ in order to satisfy a prerequisite of Lemma 1. This is accomplished by inserting the square of the common time reversal symmetry $\widehat{G}$:

$$\widehat{S} = \widehat{F}_2 \circ \widehat{G} \circ \widehat{G} \circ \widehat{F}_1 \tag{21}$$

However, $\widehat{S}$ does not formally constitute a return map for the Poincaré section $\mathcal{P}$, because as detailed in Section 2.4.1, trajectories of relevance to forward locomotion have a monotonically increasing fore-aft component; $y(t)$, hence, cannot be periodic. On the other hand, there is an effective projection informally built into the SLIP modeling assumption **P3**. At the beginning of stance, the y-coordinate of the coordinate origin must be reset to the new foothold in order to interpret $V_r$ as a radial leg potential (or, more awkwardly, one could reset the definition of the potential function at each new touchdown). Both issues can be resolved by projecting out the $y$-entry of $\widehat{S}$. A further dimensional reduction is possible because of conservation of energy in both stance and flight phase.

Formally, the total energy

$$\begin{aligned} E(\widehat{x}(t)) &= \frac{1}{2}(\dot{y}^2(t) + \dot{z}^2(t) + I\dot{\theta}^2(t)) + \\ &\quad z(t) + V(y(t), z(t), \theta(t)) \\ &=: E_0 \end{aligned}$$

can be interpreted as a constant parameter of the SLIP system and can then be used to eliminate the $\dot{y}$ variable $\dot{y}(t) = E^{-1}_{x(t)}(E_0)$,[5] with $x$ being the projection of $\widehat{x}$ onto its "non-$y, \dot{y}$" components: $\Pi : \widehat{\mathcal{X}} \to \mathcal{X}; \quad \widehat{x} \mapsto x = (z, \theta, \dot{z}, \dot{\theta})^\top$. A return map $R$ acting on the reduced Poincaré section $\mathcal{X} = \mathbb{R} \times \mathbb{S}^1 \times \mathbb{R}^2$ with independent coordinates $x$ can then be written as

$$R = \Pi \circ \widehat{F}_2 \circ \widehat{G} \circ \widehat{G} \circ \widehat{F}_1 \circ \Sigma \tag{22}$$

with

$$\Sigma : \mathcal{P} \to \widehat{\mathcal{X}}; \quad x \mapsto \begin{pmatrix} -\sqrt{1 - z^2} \\ E_x^{-1}(E_0) \\ x \end{pmatrix} \tag{23}$$

The $y$ and $\dot{y}$ components of $\widehat{F}_2$ and $\widehat{G}$ are completely decoupled from the other components, hence the projector $\Pi$ can be pulled to the right in order to define two return map factors $R_\alpha$

$$R = \underbrace{F_2 \circ G}_{=:R_2} \circ \underbrace{\Pi \circ \widehat{G} \circ \widehat{F}_1 \circ \Sigma}_{=:R_1}, \tag{24}$$

where $F_2$ and $G$ are the obvious restrictions of $\widehat{F}_2$ and $\widehat{G}$ to the reduced Poincaré section $\mathcal{X}$. If $\widehat{S}_\alpha$ are involutions, we want the involutive character to persist for $R_\alpha$. This is obvious for $R_2 = S_2$. For $R_1$ it requires $\Sigma \circ \Pi = id$ on the range of $\widehat{G} \circ \widehat{F}_1 \circ \Sigma$. Let $x_1 = \widehat{G} \circ \widehat{F}_1 \circ \Sigma(x_0)$ with $x_0 \in \mathcal{P}$. $y_1$ is the $\widehat{G}$-reflected $y$-coordinate at liftoff, hence $y_1 = -\sqrt{1 - z_1^2}$; and $\dot{y}_1 = E^{-1}_{x_1}(E_0)$. Therefore $y_1 = \Sigma \circ \Pi(y_1)$ and $R_1$ is an involution if $\widehat{S}_1$ is one.

**Controlled plant model** Having defined the closed loop return map on the reduced Poincaré section, we clarify the relation of this closed loop return map to the controlled plant model formalism introduced in Section 1.2. Since the control parameter of our SLIP model is the flight time and quantities used for feedback are the liftoff coordinates, the controlled plant model, introduced conceptually above (2), can now be written in touchdown coordinates as

$$\begin{aligned} x(k+1) &= f_2^{t_2(k)} \circ G \circ R_1(x(k)) \\ y(k) &= C(G \circ R_1(x(k))) \end{aligned} \tag{25}$$

[5] Given an equation $g(y, x) = g_0$, the corresponding implicit function will be written as $y = g_x^{-1}(g_0)$.

Using a leg angular trajectory to implement feedback control, the threshold equation implicitly defines the flight time $t_2(k)$ by

$$t_2(k) = \min_{t>0}\{t : h_2(f_2^t(G \circ R_1(x(k))), y(k), t) = 0\} \tag{26}$$

Using the explicit form of $h_2$, (19), this expression for the flight time, in turn, is a function of the control input

$$u(k) = H(y(k)) = \phi(\cdot, y(k)) \tag{27}$$

where $H$ parametrizes the leg angle trajectory in terms of the output vector $y(k)$ and the "dummy" variable $t$, denoted by $\cdot$.

### 2.4.4 Notation

The salient symbols used in this paper are next listed, with brief explanations of their meanings.

| General hybrid system definitions | |
|---|---|
| $\mathcal{I}$ | finite index set, enumerated by $\alpha$ |
| $\widehat{\mathcal{X}}_\alpha$ | chart: phase space of a dynamical system |
| $t, \widehat{x}$ | time, chart element (dimensionless) |
| $\widehat{f}_\alpha$ | vector field of a dynamical system on $\widehat{\mathcal{X}}_\alpha$ |
| $\widehat{f}_\alpha^t$ | flow of $\widehat{f}_\alpha$ on $\widehat{\mathcal{X}}_\alpha$ |
| $\widehat{F}_\alpha$ | flow map |
| $T_\alpha^\beta$ | transition function |
| $h_\alpha$ | threshold function: triggers chart transition |
| $t_\alpha(\widehat{x}_0)$ | evolution time on chart $\widehat{\mathcal{X}}_\alpha$ starting at $\widehat{x}_0$ |
| $\mathcal{P}$ | Poincaré section (surface in $\widehat{\mathcal{X}}_\alpha$) |
| $\mathcal{X}_\alpha$ | reduced Poincaré section |
| $R_\alpha$ | return map factor on $\mathcal{X}_\alpha$ |
| $R$ | return, Poincaré map |

In general, an element or a map without the diacritic $\widehat{\cdot}$ denotes an element of the reduced Poincaré section $\mathcal{X}_\alpha$ or a map on $\mathcal{X}_\alpha$.

| Other definitions | |
|---|---|
| $\widehat{G}_\alpha$ | involutive time reversal symmetry |
| $\widehat{\mathcal{X}}_{h_\alpha}$ | set where partial stride map is an involution |
| $\widehat{S}_\alpha$ | stride map factor on $\widehat{\mathcal{X}}_\alpha$ |
| $\widehat{S}$ | stride map |
| $\Pi$ | projector from $\widehat{\mathcal{X}}_\alpha$ to $\mathcal{X}_\alpha$ |
| $\Sigma$ | map from $\mathcal{X}_\alpha$ to $\widehat{\mathcal{X}}_\alpha$ |
| $V$ | conservative SLIP potential without gravity |

# 3 Stability and control of SLIP models

In this section the stability and control of SLIP models will be analyzed via the return map $R$ and its factors $R_\alpha$. In Section 3.1 it is first shown that the stance

factor $R_1$ is locally volume preserving at a fixed point $\bar{x}$, independent of the specific form of the potential $V$ as long as the conditions **P1 - P3** are satisfied. We will then derive an expression for the local volume of $R_2$ as a function of the leg angle trajectory $\phi$. Combining these two results will give a necessary condition for stability of a SLIP model in terms of the controlled leg angle trajectory $\phi$. Note that by different SLIP models we mean SLIP models that have potentials satisfying the conditions **P1** - **P3** but that differ in their leg angle trajectories $\phi$.

In the remaining portions of this section, we use the preceding analysis to explore an informal relation between the "degree of stability" as manifest in the singularity of the linearized discrete return map and the "cost of feedback." The latter is judged with respect to a number of quantitative and qualitative features of known relevance in robotic implementations. These informal "cost" measures are introduced and motivated in Section 3.2 and are shown to be quantifiable using the preceding analysis. Next, in Section 3.3 we apply the results of 3.2 to the study of several 2 DOF SLIP models (i.e., SLIP models without pitching dynamics) that have appeared in the literature, classifying them with respect to the "cost" properties previously introduced. Finally, in Section 3.4 we introduce a new 3 DOF SLIP model that offers a more realistic description of the physical robot RHex operating under the influence of its open loop gait generating "clock" [1]. We apply the analytical methods of Section 3.1, characterizing sensory "cost" and control benefit laid out in Section 3.2, and are able to give for the first time conditions on the RHex clock parameters – some necessary for gait stability, and others sufficient for gait instability.

## 3.1 Computation of the local return map volume

### 3.1.1 Stance

In this section we will apply the results of Section 2.3 to show that $R_1$ is an involution by showing that $\widehat{S}_1$ is an involution for a SLIP model satisfying the assumptions of Section 2.4.1. We first apply Lemma 2: Given $t_1 = t_1(\widehat{x}_0)$, the threshold equation in Lemma 2 reads

$$h_1(G(\widehat{x}_0), G(\widehat{x}(t_1)), t_1) = \zeta(\widehat{x}_0) - \zeta(\widehat{x}(t_1)) = 0 \quad (28)$$

However, since this is just the negative of the original threshold equation $h_1(\widehat{x}(t_1), \widehat{x}_0, t_1) = \zeta(\widehat{x}(t_1)) - \zeta(\widehat{x}_0) = 0$, $t_1$ is a solution of (28). Assuming that $t_1(\widehat{x}_0)$ is indeed the minimal solution of the threshold equation for $S_1(\widehat{x}_0)$ for all $\widehat{x}_0 \in \widehat{\mathcal{X}}$, Lemma 2 can be applied to prove that $\widehat{S}_1$ is an involution on $\widehat{\mathcal{X}}_{h_1} = \widehat{\mathcal{X}}$. By the arguments in Section 2.4.3, $R_1$ is also an involution and Theorem 3 now implies that $R_1$ is locally volume preserving at its fixed point.

### 3.1.2 Flight

We now derive a formula for the determinant of the Jacobian of the flow map $F_2$ given an arbitrary leg angle trajectory $\phi(t, x_0)$. This is used to compute the determinant of the Jacobian of the partial return map $R_2 = F_2 \circ G$ at a fixed point of $R_2$.

Note, in contrast to $R_1$, that $|\det(D_x R_2(\bar{x}))|$ can be computed directly for any specific leg angular trajectory $\phi$ using the closed form expression of the flight phase flow (17). Nevertheless, in Appendix A Lemma 2 is applied to a particular family of leg angle trajectories in order to classify which of the resulting flight phase return maps are involutions.

The threshold function $h_2$ for a general leg angle trajectory $\phi$ is $h_2(x(t), x_0, t) = z(t) - \cos(\phi(t, x_0))$ (19). Setting $h_2 = 0$ determines the time from leg liftoff ($t_{LO} = 0$) to leg touchdown $t_{TD} = t_2$. Because $h_2$ is a transcendental map, a closed form expression for $t_2(x_0)$ cannot be found in general.

It should be pointed out that the dependence of $\phi(t, x_0)$ on the flight time $t$ is redundant in the sense that the leg angle is irrelevant to the dynamics of the system except at the touchdown time $t_{TD}(x_0)$. Specifically, a given flight time $t_{TD}(x_0) = t_2(x_0)$ can be enforced by a purely state dependent leg angle "trajectory" $\phi(x_0) = \arccos(z(t_2(x_0)))$ or by any time dependent trajectory $\phi'(t, x_0)$ that satisfies

$$\phi'(t_2(x_0), x_0) = \phi(x_0) \; . \quad (29)$$

The advantage of including time as an additional argument of $\phi$ will be pointed out in Section 3.3.1.

The flow map $F_2$ takes the state vector $x_0$ from its value at leg liftoff to that at touchdown: $F_2(x_0) = x(t_{TD})$. A fixed point of a symmetric flight trajectory satisfies $\bar{x} = S_2(\bar{x}) = F_2 \circ G(\bar{x})$.

The determinant of the Jacobian of $F_2(x_0) = f_2^{t_{TD}(x_0)}(x_0)$ can easily be computed from the expression for the flight phase flow (17), bearing in mind that the flight time $t_{TD}(x_0)$ also depends on the initial conditions:

$$\det(D_x(F_2)(x_0)) = 1 - \partial_{\dot{z}_0} t_{TD}(x_0) + \dot{z}_0 \partial_{z_0} t_{TD}(x_0) + \dot{\theta}_0 \partial_{\theta_0} t_{TD}(x_0) \quad (30)$$

This expression exemplifies the remarks in Section 2.2, since it will reduce to one, in general, only if $t_{TD}$ is independent of the initial conditions $x_0$. Hence using

implicit differentiation of (19) the determinant can be written in terms of partial derivatives of $\phi(t, x_0)$:

$$\det\left(D_x F_2(x_0)\right) = 1 + \left.\frac{\Delta_2^{1\,\mathrm{num}}}{\Delta_2^{1\,\mathrm{den}}}\right|_{t=t_{TD}} \tag{31}$$

with

$$\begin{aligned}\Delta_2^{1\,\mathrm{num}} &= \sin(\phi(t,x_0)) \cdot \\ &\quad \Big(\partial_{\dot z_0}\phi(t,x_0) - \dot z_0 \partial_{z_0}\phi(t,x_0) - \dot\theta_0 \partial_{\theta_0}\phi(t,x_0)\Big) \\ &\quad + t - \dot z_0 \\ \Delta_2^{1\,\mathrm{den}} &= \sin(\phi(t,x_0))\partial_t\phi(t,x_0) - t + \dot z_0\ .\end{aligned}$$

Albeit $t_{TD}$ cannot be computed in closed form in general because of the transcendental nature of $h_2$, we know that at a fixed point $\bar x$ of $F_2 \circ G$ with $\bar x_0 := G(\bar x)$ the liftoff and touchdown heights are identical and hence $t_{TD} = 2\dot{\bar z}_0$. Therefore, $\sin(\phi(t_{TD}, \bar x_0)) = -\sqrt{1-\bar z_0^2}$ and $\theta(t_{TD}) = -\bar\theta_0$. The eigenvalues of the partial return map $F_2 \circ G$ at such a fixed point are $\{1, 1, -1, -\det(D_x(F_2 \circ G(\bar x)))\}$.

Because $G = \mathrm{diag}(1, -1, -1, 1)$, the determinant of the Jacobian of $R_2$ and $F_2$ are related as

$$\det(D_x R_2(x)) = \det(D_x F_2(G(x))) \tag{32}$$

**2 DOF SLIP model** For the 2 DOF SLIP model without pitching dynamics, the $\theta, \dot\theta$ variables are absent and $F_2$, $G$, and $R_2$ are 2-dimensional maps. The determinant of the flight phase flow map simplifies to

$$\begin{aligned}&\det(D_x F_2(x_0)) = 1 + \\ &\left.\frac{\sin(\phi(t,x_0))\left(\partial_{\dot z_0}\phi(t,x_0) - \dot z_0\partial_{z_0}\phi(t,x_0)\right) + t - \dot z_0}{\sin(\phi(t,x_0))\partial_t\phi(t,x_0) - t + \dot z_0}\right|_{t=t_{TD}}\end{aligned} \tag{33}$$

The eigenvalues of the partial return map $F_2 \circ G$ at its fixed point $\bar x$ are $\{1, -\det(D_x(F_2 \circ G(\bar x)))\}$. With $G = \mathrm{diag}(1, -1)$, the determinants of the Jacobians of $R_2$ and $F_2$ are related as

$$\det(D_x R_2(x)) = -\det(D_x F_2(G(x))) \tag{34}$$

#### 3.1.3 Local volume of the return map at a symmetric fixed point

Having derived expressions for $|\det(D_x R_1(\bar x))|$ and $|\det(D_x R_2(\bar x))|$ in the two previous sections at fixed points $\bar x$ of $R_1$ and $R_2$, the composition of $R$ of those two partial return maps $R = R_2 \circ R_1$ can be used to factor the determinant $|\det(DR(\bar x))|$ at a symmetric fixed point $\bar x$, i.e. a fixed point that is common to both $R_1$ and $R_2$ (see Section 2.3):

$$\begin{aligned}|\det(D_x R(\bar x))| &= |\det(D_x R_2(R_1(\bar x)))| \underbrace{|\det(D_x R_1(\bar x))|}_{=1} \\ &= |\det(D_x R_2(\bar x))|\end{aligned} \tag{35}$$

Hence a necessary condition for local asymptotic stability of $R$ at $\bar x$ is $|\det(DR(\bar x))| < 1$, whereas a sufficient condition for local asymptotic instability is $|\det(DR(\bar x))| > 1$.[6] The factor $|\det(D_x R_2(\bar x))|$ is governed by the time of flight (30) which in turn depends upon the functional form of the leg angle trajectory $\phi$ (31). Demanding stability of $R$ at a symmetric fixed point therefore imposes conditions on $\phi$, or, using the formalism of controlled plant models, on $H \circ C$ specified in (27).

### 3.2 Deadbeat control and singular return map Jacobians

#### 3.2.1 Control and sensor modeling

For discrete systems, three different degrees of local stability can be distinguished, which are characterized by the eigenvalues of the Jacobian of the closed loop return map at a fixed point: i) all eigenvalues are within the unit circle; ii) all eigenvalues are within the unit circle and some are zero ("singular control"); iii) all eigenvalues are zero ("deadbeat control"). In general, the more singular the closed loop return map the quicker the transient behavior[7] but the higher the "cost" of control and the more vulnerable to modeling errors. Although we are not interested in pursuing formal optimality conditions, assessing the overall sensory cost of various control alternatives is of central concern in physical robotics applications. One reasonable approach that we adopt here is to count the number and characterize the "quality" of the sensed variables required to complete the feedback loop of the controlled plant model (2). Here, "quality" refers to the frame of reference of the feedback variables, since body frame sensing is generally easier to accomplish than inertial sensing. In SLIP models, feedback control is parametrized by the leg angle trajectory $\phi(t, x_0)$, where $x_0$ are the state variables taken at a certain event. Intuitively, three different aspects of sensory cost can be readily distinguished:

**S1** Detection of the event where the feedback variables are taken
i) easy for liftoff: can be implemented in a SLIP hopper by a simple switch at the toe

[6] Note that necessary *and* sufficient conditions for stability would require the knowledge of the eigenvalues of $R$ at $\bar x$. However, eigenvalues of a composition of two maps do not factorize into eigenvalues of the two individual maps unless the maps commute - i.e., both are diagonalizable via the same similarity transformation.

[7] This is motivated by the fact that a function from $\mathbb{R}^N$ to $\mathbb{R}^N$ whose Jacobian has rank $K < N$ everywhere maps an $N$-dimensional volume to a $K$-dimensional volume.

ii) difficult for flight phase apex: requires measurement of vertical velocity $\dot{z}$

**S2** Enforcement of the angle trajectory $\phi$: a leg angle trajectory $\phi$ specified with respect to an inertial frame requires inertial sensing for enforcement (i.e. feedback control), as opposed to a leg angle trajectory specified with respect to the body frame.[8]

**S3** Sensing of the feedback variable $x_0$ by the output map $C$ (2):
i) dimension of the domain (number of arguments) of $C$
ii) position versus velocity measurement: positions are in general easier to measure than velocities
iii) "quality": inertial versus non-inertial (body frame) quantities

Because we exploit in this paper the factorization of $R$ into stance and flight phase, it is natural to work in "liftoff coordinates" – i.e., on the Poincaré section $\mathcal{P}$ – hence, the feedback variables are naturally assumed to be taken at the "easily detected" liftoff event as noted in **S1**. We appraise in Section 3.3.1 the alternative choice of working formally in apex coordinates (not to be confused with the physically unattractive choice of taking the sensory feedback measurements at the apex event). Criteria **S2** and **S3** can be addressed by rewriting the leg angular trajectory $\phi$ that is defined in an inertial frame (see Fig. 1) as

$$\phi(t, x_0) = \phi_C(t, C(x_0)) - \theta(t) \ . \tag{36}$$

The second term in (36) indicates that $\phi_C$ is specified with respect to the SLIP's body frame, as will be the case in all 3 DOF SLIP models in this paper. For 2 DOF SLIP models, $\theta$ is not defined and this term is absent.

It is not possible to distinguish **S3**iii, "quality" (i.e. inertial vs non-inertial frame based) in the 2 DOF setting, since by its very geometry, body frame coordinates cannot be introduced. On the other hand, the additional body pitch degree of freedom of the 3 DOF SLIP model allows this distinction to be made. A leg angle trajectory that only uses sensing with respect to the body reference frame **S3**, can be modeled by the following output map $C_B$ :

$$\begin{pmatrix} \phi_{B_0} \\ \dot{\phi}_{B_0} \end{pmatrix} = \begin{pmatrix} \arccos(z_0) + \theta_0 \\ -\frac{\dot{z}_0}{\sqrt{1-z_0^2}} + \dot{\theta}_0 \end{pmatrix} = C_B(x_0) \tag{37}$$

[8]Note that this feedback control cannot be modeled straightforwardly in our simplified SLIP system because of the masslessness of the leg.

where $\phi_{B0}$ is the leg liftoff angle with respect to the body normal (see Fig. 1) and $\dot{\phi}_{B0}$ is the leg's angular velocity at liftoff measured in the body frame. Specifying this trajectory in the body frame yields

$$\phi(t, x_0) = \phi_{C_B}(t, \phi_{B_0}, \dot{\phi}_{B_0}) - \theta(t) \tag{38}$$

In summary, the 3 DOF SLIP model allows the distinction of the "quality" of sensing required for a particular control input which in turn enables an assessment of the "cost" of control.

### 3.2.2 Deadbeat control requires singular return map Jacobians

In this section, we observe that deadbeat control of a 2 or 3 DOF SLIP model requires the return map Jacobian to be globally singular – not just at the control target fixed point $\bar{x}$ but on the entire reduced Poincaré section $\mathcal{X}$.

For the full nonlinear closed loop plant model the return map $R$ is deadbeat if there exists a $K \in \mathbb{N}$ such that

$$R^K(x) = \bar{x} \ \forall x \in \mathcal{X} \tag{39}$$

for a specified target $\bar{x}$. This means that

$$\begin{aligned} &D_x R(R^{K-1}(x)) \cdot D_x R(R^{K-2}(x)) \cdot \ldots \\ &\cdot D_x R(x) = 0_{\dim(\mathcal{X})\times\dim(\mathcal{X})} \qquad \forall x \in \mathcal{X} \end{aligned} \tag{40}$$

A necessary condition for this is $\det\left(D_x R(R^{K-i}(x))\right) = 0$ for some $1 \leq i \leq K$. Since eq. (40) must be valid $\forall x \in \mathcal{X}$, we need $\det\left(D_x R(x)\right) = 0 \ \ \forall x \in \mathcal{X}$.

### 3.2.3 General solution of leg angle trajectory with singular return map Jacobians

As will be reviewed in Section 3.3.1, 2 DOF SLIP models with globally singular return map Jacobians have featured prominently in the literature – both deadbeat and non-deadbeat. In this section we will derive the general form of leg angle trajectories that render the return map Jacobian globally singular. In general, the matrix $D_x F_2$ will have full rank. If, under the influence of a particular leg angle trajectory, $\phi(t, x_0)$, the second factor of the closed loop return map is rank deficient for all state vectors, $\det(D_x R_2(x_0)) = 0 = \det(D_x F_2(x_0))$, and if a stable fixed point exists, then, as discussed in Section 3.2.1, one would expect a "more rapid" convergence to this fixed point than if the matrix had full rank. Since formula (31) is valid for arbitrary flight times, not just at a fixed point of $R_2$, a partial differential equation for globally singular leg angle trajectories $\phi(t, x_0)$ can be obtained by setting (31) to zero.

First, setting eq. (30) to zero yields a partial differential equation for the touchdown time $t_{TD}$, which by the method of characteristics [31] has the general solution

$$t_{TD}(z_0, \dot{z}_0, \theta_0, \dot{\theta}_0) = t_A + \tau(z_A, \theta_A, \dot{\theta}_A) \tag{41}$$

where $\tau$ is an arbitrary differentiable function of the three arguments and the transformation from liftoff coordinates to apex coordinates is given by

$$\begin{aligned} t_A &= \dot{z}_0 \\ \dot{\theta}_A &= \dot{\theta}_0 \\ z_A &= z_0 + \frac{\dot{z}_0^2}{2} \\ \theta_A &= \theta_0 + \dot{\theta}_0 \dot{z}_0 \end{aligned} \tag{42}$$

specifying the time from liftoff to apex, the pitching velocity at apex, the apex height, and the apex pitch angle. Since a scalar function $t_{TD}$ is determined by this partial differential equation, the rank of $D_x F_2$ will generally be reduced by only one using $t_A + \tau(z_A, \theta_A, \dot{\theta}_A)$ as the flight time.

Now recall that the time of flight function, $t_{TD} = t_2$ arises in our application as the solution of an implicit function defined by the leg angle trajectory $\phi$ (19). Thus, we must next impose a corresponding "singularity" condition on $\phi$ that guarantees the desired property in $t_{TD}$. Setting eq. (31) to zero, $\det(DF_2(x_0)) = 0$, yields the partial differential equation for globally singular leg angle trajectories,

$$\partial_t \phi(t, x_0) + \partial_{\dot{z}_0} \phi(t, x_0) - \dot{z}_0 \partial_{z_0} \phi(t, x_0) - \dot{\theta}_0 \partial_{\theta_0} \phi(t, x_0) = 0$$

The general solution of this linear, homogeneous, first order partial differential equation by the methods of characteristics is

$$\phi(t, x_0) = \Phi(t - t_A, z_A, \theta_A, \dot{\theta}_A) \tag{43}$$

where $\Phi$ is an arbitrary differentiable function of its four arguments.

## 3.3 2 DOF SLIP models: sensor requirements and stability

This section focuses on 2 DOF SLIP models with respect to sensor requirements in their feedback loop. First, it is shown that all 2 DOF SLIP models with globally singular return map Jacobians require a measurement of the vertical velocity, either explicitly through the arguments of $\phi$ or implicitly. Then the dimensional reduction of the return map that follows from the globally singular return map Jacobians is illustrated with four different 2 DOF SLIP models that have already appeared in the literature. A stable 2 DOF SLIP model with full rank return map Jacobian is also presented to illustrate the power of our analysis in the low dimensional setting. Since the reduced Poincaré section, $\mathcal{X}$, is only two dimensional for the 2 DOF model, the presence of complex conjugate eigenvalues of the linearized return map at a given fixed point strengthens our stability criteria to the point that the determinant magnitude condition is both necessary and sufficient for asymptotic stability. Thus, as we demonstrate, by varying one parameter, asymptotically stable, neutrally stable, and unstable behavior can be exactly assigned.

### 3.3.1 All singular 2 DOF SLIP models require velocity sensing

In this section several previously proposed [13, 14, 9, 32, 33] 2 DOF SLIP control strategies are reviewed with emphasis on their globally singular return map Jacobians. The general solution for a globally singular leg angle trajectory for the 2 DOF SLIP model is obtained from (43) by omitting the pitch coordinates, hence $\phi(t, x_0) = \Phi(t - t_A, z_A)$. But both control input arguments require the vertical velocity measurement $\dot{z}_0$ when expressed in liftoff coordinates (42), which leaves the constant trajectory $\phi(t, x_0) = const$ as the only globally singular leg angle trajectory without explicit velocity sensing. We will review four 2 DOF SLIP models with globally singular leg angle trajectories, pointing out that even the leg angle trajectory $\phi(t, x_0) = const$ requires velocity sensing for its implementation as highlighted in criterion **S2**.

**Constant leg touchdown angle policy** The constant leg touchdown angle policy proposed in [13, 14, 34, 32] has the simple form

$$\phi(t, x_0) = 2\pi - \beta \quad : t > t_A \tag{44}$$

where $\beta$ is a constant angle for all strides. No sensing of the feedback variables **S3** is required, hence the output map $C$ can be taken to be a constant. Since the return map Jacobian of this SLIP model is globally singular, the return map is effectively one-dimensional. In [13] this one-dimensional variable was taken to be the apex height, whereas in [14] the angle of the touchdown velocity was chosen.[9]

[9] A similar leg angular trajectory for a 3 DOF SLIP model was shown in [14] to yield asymptotically stable behavior for certain parameter values. Although not presented here, the return map factorization introduced in this paper can be applied to this model also to show that its stance phase is locally volume preserving at a symmetric fixed point whereas its flight phase has a globally singular return map.

A Poincaré section volume and the embedded one-dimensional return map domain is plotted in Fig. 2a), where the return map image $\mathcal{X}^I := R(\mathcal{X})$ with $\mathcal{X} = [0.8, 0.99]\times[-1.5, -0.1]$ is depicted by solid points joined by a black line. The color of the points matches the color of the inverse images $R^{-1}\left(\mathcal{X}^I(z_{A_i})\right)$ of these points. The color corresponds to a parametrization of the return map image in terms of the resulting apex heights $z_{A_i}$. Since a constant leg touchdown angle is prescribed, the touchdown height is constant and the return map image is a vertical line in $(z_0, \dot{z}_0)$-coordinates. The curved black line denotes the one-dimensional manifold of all possible fixed points for arbitrary leg angle trajectories.[10] Although $\phi$ is a constant and does not explicitly depend on the velocity measurement of $\dot{z}_0$, vertical velocity sensing is implicit in the derivation of the return maps in [13, 14, 34, 32], because the leg angle is not held constant throughout the flight phase, but is assumed to be set to $2\pi-\beta$ in a time interval $(\dot{z}_0-\sqrt{\dot{z}_0^2+2(z_0-\sin\beta)}, \dot{z}_0+\sqrt{\dot{z}_0^2+2(z_0-\sin\beta)})$ in which the COM is above the touchdown height $\sin\beta$. Before this time interval is reached, the leg is assumed to be at an angle where it does not interfere with the ground.

**Raibert controller** The leg placement strategy proposed by Raibert [9] for a two degree of freedom SLIP reads

$$\phi(t, x_0) = 2\pi - \arcsin\left(\frac{\dot{y}_0 t_s}{2} + k_{\dot{y}}(\dot{y}_0 - \dot{\bar{y}})\right) \qquad (45)$$

where $t_s$ is the duration of the stance phase, $k_{\dot{y}}$ is a feedback gain and $\dot{\bar{y}}$ is the desired forward speed. In Raibert's physical implementations, the duration of the current stance phase was approximated by the measured duration of the previous stance phase. Here, we will consider $t_s$ a constant. In (45) the average forward stance speed used in [9] was approximated by $\dot{y}_0$. Now $\dot{y}_0$ can be expressed as $\dot{y}_0 = \sqrt{2(E - z_A)}$. Hence eq. (45) is of the form (43) and the return map domain is a one-dimensional manifold which is depicted in Fig. 2b). The output map for this leg angular trajectory reads $C(x_0) = z_A$.

**Leg retraction and "optimized selfstabilization"** In the leg retraction schemes proposed in [15, 33], the leg is set at a fixed angle $\alpha_A$ at the apex of the flight phase and then starts rotating towards the ground. Before reaching the apex, the leg angle can be arbitrarily placed as long as its toe does not touch the ground. In [15], a constant angular velocity $\omega$ is used (leg retraction), i. e.

$$\phi(t, x_0) = \alpha_A + \omega(t - t_A) \quad : t > t_A \qquad (46)$$

whereas in [33] a nonlinear angular trajectory that is constant over all strides

$$\phi(t, x_0) = \alpha(t - t_A) \quad : t > t_A \qquad (47)$$

is employed. In both cases, the output map is $C(x_0) = t_A$. Clearly, these two leg placement schemes are also of the form (43) and therefore the return map image is a one-dimensional manifold. These return map images are plotted in Figs. 2c and d respectively. Both return maps converge to the same point, however, the second trajectory [33] achieves convergence to a desired apex height within one stride.[11] Since the apex Poincaré section in [33] is only one-dimensional and one control parameter – the touchdown time or rather the leg touchdown angle – is available, the desired apex height can be reached within one stride. On the other hand, the touchdown Poincaré section parametrized by $(z, \dot{z})$ is two-dimensional and deadbeat control can only be achieved within at least two strides. This seems to be a contradiction, since the discrete time behavior of identical physical systems parametrized by different Poincaré sections must be conjugate, i.e. related by a coordinate transformation. Particularly the dimension of the return maps of both parametrizations must agree. In Appendix B it is shown that if all coordinates of the dynamical flow are taken into account, the apex and touchdown return maps are indeed conjugate. However, because the open loop system is dynamically decoupled in apex coordinates (i.e. the second variable does not influence the evolution of the first in these coordinates), restricting the feedback to depend upon the first variable yields effectively a one-dimensional closed loop return map. This one-dimensional nature is illustrated in Fig. 2d), where the one-dimensional manifold $\mathcal{X}^I := R(\mathcal{X})$ is plotted together with color-coded inverse images $R^{-1}\left(\mathcal{X}^I(z_{A_i})\right)$. As can be seen in Fig.

[10] By Theorem 2 a fixed point of the time reversed stance flow map $\widehat{S}_1$ lies on a symmetric orbit of its vector field $\widehat{f}_1$. Symmetric orbits must contain a fixed point of $\widehat{G}$ [30] and can therefore be characterized for the 2 DOF SLIP model by the two-dimensional fixed point set $\mathrm{Fix}\widehat{G} = \{\widehat{x} \in \widehat{\mathcal{X}} : y = 0, \dot{z} = 0\}$. Fixing the energy $E_0$ removes one dimension, hence the set of all possible fixed points of the return map factor $R_1$ forms a one-dimensional manifold in $\mathcal{X}$. Given that any $x = (z, \dot{z})^\top$ with $\dot{z} > 0$ lies on a symmetric orbit of the flight phase vector field $f_2$ on the reduced Poincaré section $\mathcal{X}$, the set of all possible fixed points of the return map $R$ is identical to the one-dimensional manifold of possible fixed points of $R_1$. The fixed points of $R$ are then given by the intersection of this line with the return map image.

[11] The angular trajectory $\alpha$ was obtained by numerical inversion of the apex height-to-apex height return map in order to implement deadbeat control.

2d, $\mathcal{X}^I$ is aligned with one of the inverse images, hence in the first stride an arbitrary point $(z, \dot{z})$ is mapped onto $\mathcal{X}^I$, whereas in the second stride all points on this manifold are mapped to the target point.

The authors of [33] call this control scheme "optimized selfstabilization," indicating a computational or sensory advantage over regular deadbeat control. In regular deadbeat control, the leg angle $\phi$ would be a function of both $z_0$ and $\dot{z}_0$, requiring the sensing of both liftoff variables and the online computation or storage of a lookup table for a function from a two-dimensional to a one-dimensional space. In (47) only the sensing of $t_A = \dot{z}_0$ and a clock is required, and $\alpha$ is a function from a one-dimensional to a one-dimensional space. In this context, "selfstability" seems to refer to the fact that the leg angle is a function of time (starting at apex) only and and does not explicitly depend upon the liftoff variables $(z_0, \dot{z}_0)$; it does not mean that no sensing (e. g. detection of the apex) is required. In the next paragraph we address the explicit parametrization of this one-dimensional return map manifold and show how it can be used to reduce the sensory requirements of control.

**Sensory requirements of globally singular control:** Given a globally singular 2-DOF SLIP return map with leg angle trajectory $\phi(t, x_0)$, this leg angle trajectory can be rewritten as $\phi(t, x_0) = \Phi(t - t_A, z_A)$ according to the results in section 3.2.3. The corresponding output map can be chosen to be $C(x_0) = (t_A, z_A)^\top$. This does not constitute a sensory advantage over $x_0$ because still one position and one velocity measurement are required. The threshold function reads

$$\begin{aligned} h_2(x(t), x_0, t) &= z(t) - \cos\left(\Phi(t - t_A, z_A)\right) \qquad (48) \\ &= z_A - \frac{(t - t_A)^2}{2} - \cos\left(\Phi(t - t_A, z_A)\right) \end{aligned}$$

Setting $h_2$ to zero implicitly defines a function $\Delta t_A$ with the substitution $t - t_A \to \Delta t_A(z_A)$. $\Delta t_A(z_A)$ encodes the direct control parameter during flight – the total flight time $t_A + \Delta t_A(z_A)$. A different angular trajectory enforcing the same total flight time for all initial conditions $z_0, \dot{z}_0$ can then be defined by the inverse $\Delta t_A^{-1}$: $\hat{\Phi}(t - t_A) := \Phi(t - t_A, \Delta t_A^{-1}(t - t_A))$ with a new output map $C(x_0) = t_A$ whose only output is the flight time measured from apex. Hence a leg angle trajectory $\phi(t, x_0)$ that initially required the sensing of $(t_A, z_A)^\top$ and time can be replaced by one that only requires sensing of the apex, i. e. $t_A = \dot{z}_0$, and time. This rewriting of the angular trajectory makes use of the invariance of the flight time with respect to certain parametrizations of $\phi$ (29) and demonstrates why deadbeat control for SLIP models can be achieved with reduced feedback sensing **S3**i.

### 3.3.2 A nonsingular, stable 2 DOF SLIP model without velocity sensing

We will now investigate a 2 DOF SLIP model with a full rank return map Jacobian where we address both **S3**i and **S3**ii in that no velocity sensing is required for the feedback loop. For certain parameter values, this model does exhibit asymptotic stability. In the previous 2 DOF examples of Section 3.3.1, once singularity has been imposed, the determinant of the return map Jacobian vanishes and the factor analysis can contribute no more information to the stabilization problem. However, as this example shows, since the return map has dimension two, if we operate in a regime where the eigenvalues are known to have nonzero imaginary components, then the properties of the determinant completely determine stability. We can then dictate the stability properties through a closed form expression and this is indeed how the present example has been adjusted.

The leg angle trajectory for this model reads

$$\phi(t, x_0) = \omega t + k \arccos(z_0) + \alpha_A \qquad (49)$$

where $\omega, k$, and $\alpha_A$ are constants. Note that $\dot{z}_0$ does not appear in (49), hence the output map could be written as $C(x_0) = z_0$. For $k = 1$ and $\alpha_A = 0$, the leg rotates clockwise at a constant rate $\omega$ starting with the liftoff angle $\arccos(z_0)$. This can be considered a crude 2 DOF SLIP version of the leg angle profile specified by RHex's open loop controller [1]. A more elaborate 3 DOF SLIP version of RHex's open loop controller will be presented in Section 3.4.2. Using (33) the determinant of the Jacobian of $R$ at a symmetric fixed point becomes:

$$\begin{aligned} |\det(D_x R(\bar{x}))| &= |\det(D_x F_2(G(\bar{x})))| \\ &= |1 + \frac{-\dot{\bar{z}}(k-1)}{-\dot{\bar{z}} + \omega\sqrt{1-\bar{z}^2}}| \qquad (50) \\ &\quad \begin{cases} < 1 & : \quad \frac{\omega\sqrt{1-\bar{z}^2}}{\dot{\bar{z}}} < k < 1 \\ = 1 & : \quad k = 1 \\ > 1 & : \quad k > 1 \end{cases} \end{aligned}$$

In order to illustrate the predictive power of (50), we numerically approximate the determinant $\det(D_x R(\bar{x}))$ of the full return map for fixed SLIP parameters $E_0 = \frac{\tilde{E}_0}{\tilde{m}\tilde{g}\tilde{\zeta}_0} = 2.1$, $\gamma = 13$, and fixed recirculation parameters $\alpha_A = \pi$, $\omega = 14$ for different $k \in \{1/6, 0.5, 1, 2, 3.3\}$. Here, $E_0$ is the dimensionless total conserved energy of the system and the dimensionless spring potential is $V(\zeta) = (\gamma/2)(\zeta - 1)^2$. We

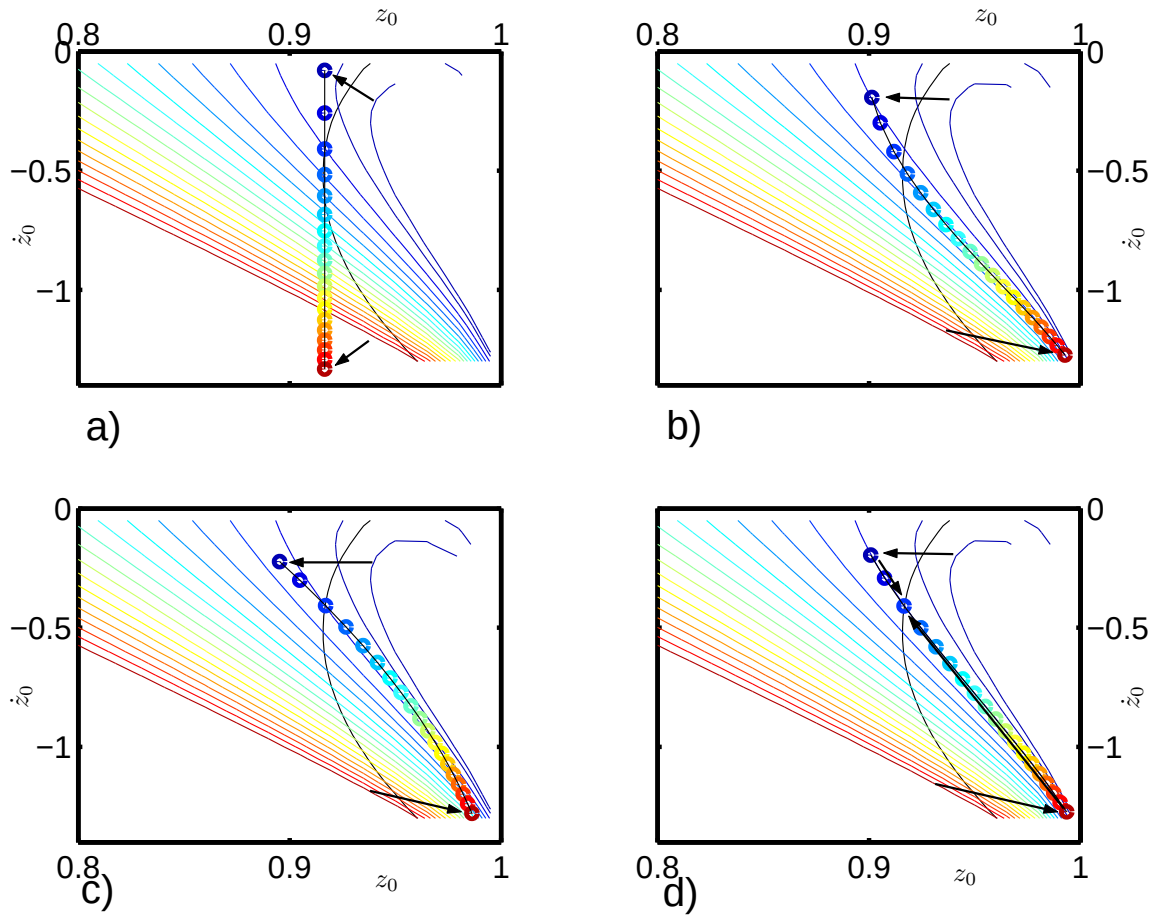


Figure 2: One-dimensional return map domains and their inverse images for rank-deficient SLIP-controllers: a) Fixed leg angle touchdown, b) Raibert, c) Leg retraction, d) Two-step deadbeat. All elements of a colored line in the $(z_0, \dot{z}_0)$-plane are mapped to the point with identical color. The union of all these points constitutes the return map image. The color corresponds to a parametrization of the return map image in terms of the resulting apex heights $z_{A_i}$. The range of apex heights considered is $z_A \in [0.92, 1.8]$. The curved black line identical in all four figures denotes the set of all possible fixed points, as explained in Footnote 10.

then compare these values to the values of the determinant obtained by inserting the numerically determined fixed points $\bar{x} = (\bar{z}\ \dot{\bar{z}})^\top$ into (50). The determinants obtained in those two different ways are plotted in Fig. 3a and agree to a high precision ($||\det(D_x R(\bar{x}))| - |\det(D_x F_2(G(\bar{x})))|| < 10^{-7}$). In Figs. 3b-d iterations of the return map in $(z_0\ \dot{z}_0)$-space are shown for $k \in \{1/6, 1, 3.3\}$ and initial conditions off the fixed point. The eigenvalues are complex conjugate pairs in all three cases, hence, the magnitude of the eigenvalues computed in (50) specifies sufficient as well as necessary conditions for stability and instability in this case. For $k = 3.3$, formula (50) specifies an unstable fixed point, and, indeed, the plot of a numerical simulation in Fig. 3b depicts a typical trajectory spiraling away from a small neighborhood as required.

For $k = 1/6$, formula (50) specifies asymptotic stability, and trajectories spiral towards the fixed point, as depicted in Fig. 3c. For $k = 1$, formula (50) suggests neutral stability and numerical simulation verifies that all trajectories lie on deformed circles around the fixed point as plotted in Fig. 3d.

Fig. 3d is reminiscent of KAM-tori of area-preserving 2D mappings (see [35]), however, as can be seen in Fig. 4, the phase space volume is not preserved away from the fixed point $\bar{x}$ for $k = 1$. In Appendix C we invoke reversibility [36] in place of area-preservation to show that the numerically observed neutral stability for the leg recirculation scheme with k = 1 is expected.

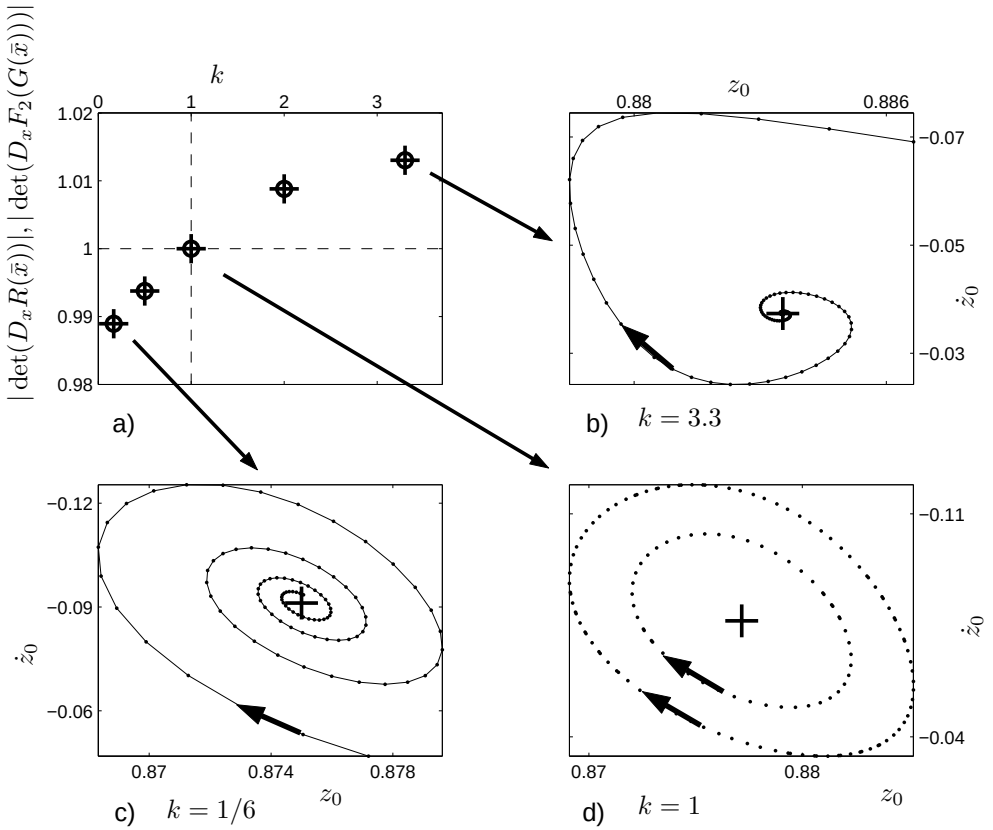


Figure 3: a) Comparison of the numerically computed determinant $|\det(D_xR(\bar{x}))|$ (+) of the return map Jacobian to to the determinant $|\det(D_xF_2(G(\bar{x})))|$ (∘) obtained by using the numerically determined fixed points in (50). b)-d) Trajectories around a fixed point. Because of slow convergence, only every 9th iteration in plot b) and every 5th iteration in plot c) is shown.

## 3.4 3 DOF SLIP models: body-frame sensing and stability

In this section the control possibilities with body frame sensing are explored for 3 DOF SLIP models. First, the unique 3 DOF SLIP model with the body frame sensor model (37) and a globally singular return map Jacobian is presented. By comparing the number of available design parameters of this SLIP model to the dimension of the reduced Poincaré section, deadbeat control is excluded. Then a nonsingular 3 DOF SLIP model with only body frame sensing is introduced. It is modeled within the limitations of the 3 DOF SLIP dynamics after the open-loop controller of RHex [1] and is shown to have asymptotically stable operating regions. A necessary condition for the stability of this model in terms of a RHex clock parameter is derived.

### 3.4.1 Body frame sensing does not admit deadbeat control

We want to investigate the possibility of deadbeat control with a leg angle trajectory of the form (38) $\phi(t, x_0) = \phi_{C_B}(t, \phi_{B_0}, \dot{\phi}_{B_0}) - \theta(t)$, i.e. using only body fame sensor information in the feedback loop and specifying the leg angle trajectory in the body frame.

As shown in Section 3.2.2, deadbeat control requires globally singular return map Jacobians and hence $\phi_{C_B}(t, \phi_{B_0}, \dot{\phi}_{B_0}) - \theta(t)$ must be cast into the form $\Phi(t-t_A, z_A, \theta_A, \dot{\theta}_A)$ (43). While $\theta(t) = \theta_A + \dot{\theta}_A(t-t_A)$ does satisfy this functional form, $\phi_{C_B}(t, \phi_{B_0}, \dot{\phi}_{B_0})$ does not, except for $\phi_{C_B}(t, \phi_{B_0}, \dot{\phi}_{B_0}) = const.$ We will present numerical evidence in the form of an asymptotically stable trajectory at particular parameter values of a 3 DOF SLIP model in order to show that stable behavior is possible with the leg angle trajectory

$$\phi(t, x_0) = 2\pi - \beta - \theta(t) \ . \tag{51}$$

This 3 DOF SLIP model bears close resemblance to the LLS model [11] of horizontal legged locomotion, where at the end of each stance phase the new stance

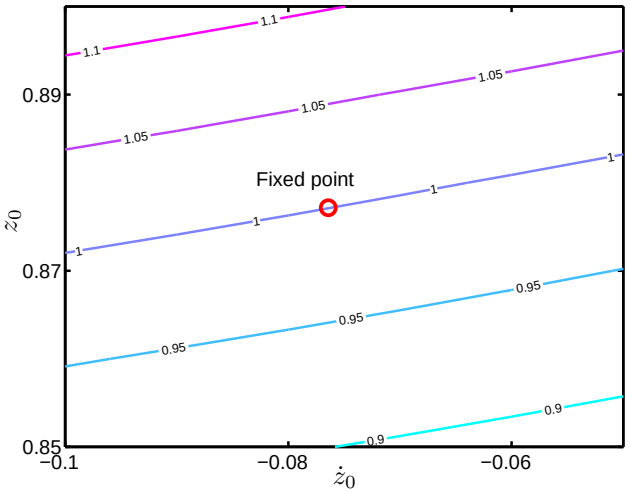


Figure 4: Contour plot of $|\det(D_x R(\bar{x}))|$ for the leg angle trajectory (49) with $k = 1$. The fixed point $\bar{x} \approx (0.8772, -0.0764)^\top$ lies on the $|\det(D_x R(x))| = 1$ contour, whereas volume (area) is not preserved away from the fixed point.

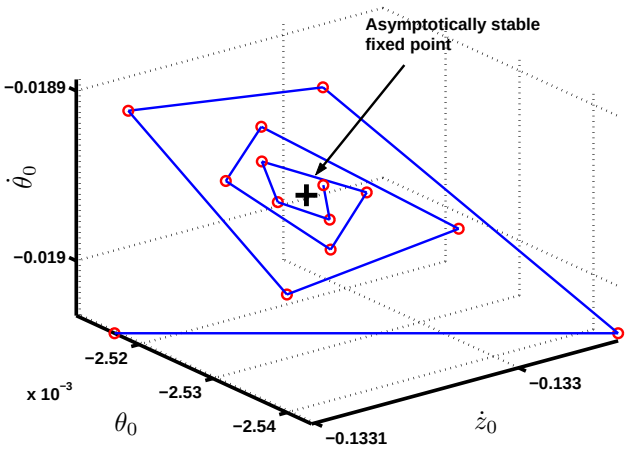


Figure 5: A sample discrete trajectory on the 3-dimensional Poincaré section parametrized by $(\dot{z}_0, \theta_0, \dot{\theta}_0)$ converging to an asymptotically stable fixed point. Because of the rank-deficient nature of the leg placement, $z_0$ is a function of the other Poincaré section variables $z_0 = \cos(\theta_0 + \pi/2 - \beta)$. The values of the dimensionless variables characterizing this system are $c_{\theta\theta} = 400$, $c_{\theta\psi} = -12$, $c_{\psi\psi} = 0$, $E_0 = 2.1$, $\gamma = 13.25$, $I = 0.489$, and $\beta = 1.0562$.

leg is set at a fixed angle with respect to the non-inertial body axis, thus implementing a similar leg angular trajectory.[12] A sample discrete trajectory on the 3-dimensional Poincaré section is shown in Fig. 5 for a potential of the form **P3** with $V_r(\zeta) = (\gamma/2)(\zeta - 1)^2$ and $V_p(\psi, \theta) = 1 + c_{\theta\theta}\theta^2 + c_{\theta\psi}\theta\psi + c_{\psi\psi}\psi^2$. The motivation for this potential is discussed in Section 4.1. Given that the only design parameter of (51) is $\beta$, a target point $(\dot{\bar{z}}, \bar{\theta}, \dot{\bar{\theta}})$ in the reduced three-dimensional Poincaré space cannot be specified a priori. Hence the possibility of deadbeat control for the 3 DOF SLIP model with the body frame sensor model (37) must be discarded.

### 3.4.2 A RHex-like 3 DOF SLIP model with body frame sensing

In this section a leg placement strategy for the control of the 3 DOF SLIP model with full rank is investigated. Its importance lies in the fact that this leg placement strategy is modeled after the open-loop controller employed in RHex [1] within the limitations of the 3 DOF SLIP model. The angular reference trajectories prescribed by RHex's open loop clock controller [1] are specified by the (dimensionless) parameters $t_c, t_s, \varphi_s, \varphi_0$; see Fig. 6. For one half of the clock period $t_c$, the trajectories for the left (L) and the right (R) tripod can be expressed as functions of time in the robot's body frame (B) as

$$\phi_{B_L}(t) = \begin{cases} \omega_s t + \varphi_0 & 0 \le t < \frac{t_s}{2} \\ \omega_f t + \frac{\varphi_s}{2}(1 - \frac{\omega_f}{\omega_s}) + \varphi_0 & \frac{t_s}{2} \le t < \frac{t_c}{2} \end{cases} \tag{52}$$

$$\phi_{B_R}(t) = \begin{cases} -\pi + \omega_f t + \varphi_0 & 0 \le t < \frac{t_c - t_s}{2} \\ \omega_s t - \frac{\varphi_s}{2}(1 - \frac{\omega_s}{\omega_f}) - \pi\frac{\omega_s}{\omega_f} + \varphi_0 & \frac{t_c - t_s}{2} \le t < \frac{t_c}{2} \end{cases}$$

where $\omega_s = \frac{\varphi_s}{t_s} < \omega_f = \frac{2\pi - \varphi_s}{t_c - t_s}$. These angular trajectories are depicted in Fig. 6. They are enforced at each leg of the robot by a simple PD-controller.

In order to implement this controller in a simplified 3 degree of freedom SLIP controller, the following assumptions are made:

**R1** RHex's clock should prescribe motions with (substantial) flight phases, i.e. $t_s < t_c/2$.

**R2** During stance the (virtual) stance leg can be approximated by a SLIP; this means that there is no net torque apart from gravity on the leg.

**R3** The PD-controller that enforces the angular reference trajectories (52) during flight has infinite gains and tracks those trajectories without errors. In consequence, as the present stance leg lifts off,

[12] Note, however, that the flight duration is zero.

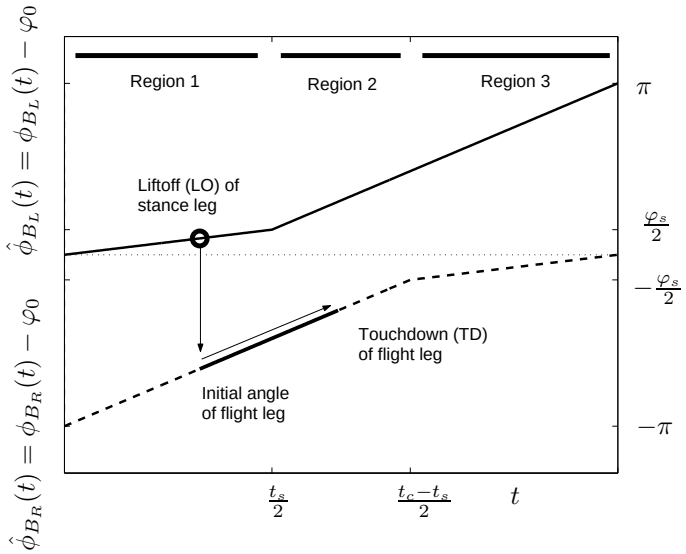


Figure 6: Illustration of liftoff and touchdown events in the body frame of a RHex-inspired leg recirculation scheme [1] for SLIP with pitching dynamics.

the PD-controller can be assumed to have positioned the second (present flight) leg at the exact angle with respect to the first (present stance) leg as specified by (52). In contrast, during stance, the angular position and velocity variables evolve according to the SLIP stance mechanics (13).

Assumption **R1** simply focuses attention on RHex's dynamical regime as opposed to the possibly quasi-static operation available to platforms with sufficiently high leg number. Assumption **R2** is justified by experiments and simulation studies of RHex operating in the relevant dynamical regime [37, 2, 34]. Assumptions **R2** and **R3** make the controlled SLIP model a pseudo-clock controlled system, where the clock signal is turned off during stance and turned on at a reset phase at liftoff. In the following derivation, the left leg (L) is chosen to be the stance leg.

In order to cast the reference trajectories in an expression for $\phi(t, x_0)$ using assumption **R3** we need to express $\phi_{B_R}$ (the flight leg angle with respect to the body frame) in terms of the angle of the stance leg at liftoff $\phi_{B_L}(t_{LO})$.[13] In addition, we need to transform leg angles specified in the body frame to the respective angles in the inertial frame. The relation between the body and the inertial frame is given by

$$\phi_B = \phi + \theta \tag{53}$$

Hence the leg angle trajectory of the right (flight) leg with respect to the inertial frame is given by

$$\phi_R(t) = \phi_{B_R}(t + t_{LO}) - \theta(t) = \phi(t, x_0) \tag{54}$$

where $t_{LO} = \phi_{B_L}^{-1}(\phi_{L_0} + \theta_0)$ is the time with respect to the RHex clock when liftoff occurs and $\phi_{L_0} = \arccos(z_0)$ is the angle of the stance leg at liftoff in the inertial frame. This procedure is illustrated within the body frame in Figure 6.

Using the expressions for the RHex clock trajectory (52), we obtain an angular trajectory for the 3 DOF SLIP system that at any instant in time has the general form

$$\phi(t, x_0) = \omega t + k \underbrace{(\arccos(z_0) + \theta_0)}_{=\phi_{B_0}} + \alpha_A - \theta(t) \tag{55}$$

with $\omega \in \{\omega_f, \omega_s\}$, and $k \in \{\frac{\omega_s}{\omega_f}, 1, \frac{\omega_f}{\omega_s}\}$; the different values of $\alpha_A$ can easily be derived and are not important in this context. This expression is of the form (38) with the body frame sensor model $C_B(x_0) = \arccos(z_0) + \theta_0 = \phi_{B_0}$, i.e. no body frame velocity measurement is required. The functional form of eq. (55) translates into different functional expressions for $|\det(DF_2(G(\bar{x})))|$ which are distinguished by the location of liftoff and touchdown with respect to the piecewise-linear leg angle trajectories. We enumerate these six cases by two numbers (LO $\rightarrow$ TD) which denote the region in Fig. 6 where liftoff and touchdown occurs.

| (LO $\rightarrow$ TD) | $\lvert\det(DF_2(G(\bar{x})))\rvert$ |
|---|---|
| $(1 \rightarrow 1)$<br>$(1 \rightarrow 2)$ | $\lvert 1 + \frac{(-\dot{\bar{z}} + \dot{\bar{\theta}}\sqrt{1-\bar{z}^2})(\frac{\omega_f}{\omega_s} - 1)}{(-\dot{\bar{z}} + \dot{\bar{\theta}}\sqrt{1-\bar{z}^2}) + \omega_f\sqrt{1-\bar{z}^2}} \rvert \overset{\dot{\bar{\theta}} > \frac{\dot{\bar{z}}}{\sqrt{1-\bar{z}^2}}}{>} 1$ |
| $(2 \rightarrow 2)$<br>$(1 \rightarrow 3)$ | 1 |
| $(2 \rightarrow 3)$<br>$(3 \rightarrow 3)$ | $\lvert 1 + \frac{(-\dot{\bar{z}} + \dot{\bar{\theta}}\sqrt{1-\bar{z}^2})(\frac{\omega_s}{\omega_f} - 1)}{(-\dot{\bar{z}} + \dot{\bar{\theta}}\sqrt{1-\bar{z}^2}) + \omega_s\sqrt{1-\bar{z}^2}} \rvert \overset{\dot{\bar{\theta}} > \frac{\dot{\bar{z}}}{\sqrt{1-\bar{z}^2}}}{<} 1$ |

Table 1: Functional expressions for $|\det(DF_2(G(\bar{x})))|$ for different locations of the liftoff and touchdown event.

Based on the properties of symmetric orbits that we focus on in this paper, a necessary condition on a RHex clock parameter for asymptotic stability can now be derived.

**A necessary condition for asymptotic stability**
For symmetric orbits, the liftoff and touchdown leg angles in the inertial frame are of equal magnitude but opposite sign: $\phi_{L_0} = -\phi_R(t_{TD})$. This also holds for the pitching angles: $\theta_{L_0} = -\theta(t_{TD})$. Using (53) to

[13] Note that the time in $\phi_{B_L}$ differs from the time in $\phi(t, x_0)$; it is not reset at the beginning of a new flight phase.

translate the liftoff and touchdown angles to the body frame

$$\begin{aligned}\phi_{B_L}(t_{LO}) &= \phi_{L_0} + \theta_{L_0} \\ \phi_{B_R}(t_{TD}) &= \phi_R(t_{TD}) + \theta(t_{TD})\end{aligned}$$

we obtain $\phi_{B_L}(t_{LO}) + \phi_{B_R}(t_{TD}) = 0$. With the definitions $\hat{\phi}_{B_L} = \phi_{B_L} - \varphi_0$ and $\hat{\phi}_{B_R} = \phi_{B_R} - \varphi_0$ as in Figure 6, this equality can be rewritten as

$$\hat{\phi}_{B_L}(t_{LO}) + \hat{\phi}_{B_R}(t_{TD}) = -2\varphi_0 \tag{56}$$

By locating the liftoff and touchdown angles of (56) for symmetric orbits within regions 1-3 in Figure 6, a table of possibly allowed liftoff-touchdown transitions as a function of the sign of RHex clock's leg offset angle $\varphi_0$ can be derived:

| (LO → TD) | $\varphi_0 < 0$ | $\varphi_0 = 0$ | $\varphi_0 > 0$ |
|---|---|---|---|
| $(1 \to 1)$<br>$(1 \to 2)$ | no | no | yes |
| $(2 \to 2)$<br>$(1 \to 3)$ | yes | yes | yes |
| $(2 \to 3)$<br>$(3 \to 3)$ | yes | no | no |

If $\dot{\bar{\theta}} > \frac{\dot{\bar{z}}}{\sqrt{1-\bar{z}^2}}$, the determinant for the transitions $(2 \to 3)$ and $(3 \to 3)$ will be less than one. Hence a necessary condition for asymptotic stability is $\varphi_0 < 0$ provided that $\dot{\bar{\theta}} > \frac{\dot{\bar{z}}}{\sqrt{1-\bar{z}^2}}$. On the other hand, a sufficient condition for instability (including neutral stability) is $\varphi_0 > 0$ provided that $\dot{\bar{\theta}} > \frac{\dot{\bar{z}}}{\sqrt{1-\bar{z}^2}}$.

It should be emphasized that the expressions in table 1 are independent of the specific 3 DOF SLIP potential $V$ as long as the general conditions **P1** - **P3** listed in 2.4.1 are obeyed. However, a specific SLIP model does influence the location of fixed points $\bar{x}$ and therefore the numerical value of the determinant for the cases $1 \to 1, 1 \to 2, 2 \to 3, 3 \to 3$ as well as the location of the eigenvalues.

This analysis provides for the first time a partial explanation for the surprising stability of the open-loop clock driven robot RHex.

# 4 Application: Toward hierarchical control of a hexapedal robot

In this section we explore numerically the applicability of these ideas to the robot RHex [1]. In Section 4.1 we review the general approach to hierarchical control [5] in the specific context of a RHex-like anchor system compared to the SLIP-template with a physically motivated stance phase potential and leg angle trajectory. In Section 4.2 we present simulation results and assess the degree of correspondence between the simulated anchor and its putative template.

## 4.1 Control of the anchor by controlling the template

A template is a low dimensional model of a mechanism operating within a specified environment that is capable of expressing a specific task. To anchor this low dimensional model in a more physically realistic higher degree of freedom representation of the robot and its environment, we seek controllers whose closed loops result in a "prescriptive" correspondence (defined in Section 1.2) of the dynamics of the high and low degree of freedom models. Hence the controller must a) force the high-dimensional anchor to follow the dynamics of the low-dimensional template ("anchoring"), and b) control the template to achieve a certain task. In the case at hand the anchor is given by the robot RHex, whereas the template is given by a 3 DOF SLIP model as in Section 2.4.1 with a leg angle trajectory (55). Note that this template-anchor hierarchy includes the intrinsic abstraction of neglecting lateral dynamics and focusing on the sagittal plane motion. The analysis of the previous chapters will be shown to give insights into part b); we assume that the SLIP-anchoring mechanism (part a)) has already been addressed by either deliberate design [6] or by the interaction of the controlled robot with its environment, as has been shown for RHex's steady state behavior [37, 2].

As a first step towards the goal of devising a new controller for RHex or optimizing RHex's open loop controller, we provide numerical evidence for the agreement of the stability properties of a RHex-like model programmed in the SimSect simulation environment [7] with the stability properties of the 3 DOF SLIP model introduced in Section 3.4.2. In particular, we show that in a physically interesting operational regime, stable simulations in SimSect correspond to stable fixed points of the corresponding SLIP model.

Here, "correspondence" is established by fitting simulation data to the 3 DOF SLIP model with stance phase potential introduced in Section 3.4.1 and with the RHex-like leg angle trajectory (55) using the RHex clock parameters of the SimSect simulation. This

stance phase potential

$$V(y,z,\theta) = \frac{\gamma}{2}(\zeta-1)^2\left(1 + c_{\theta\theta}\theta^2 + c_{\theta\psi}\theta\psi + c_{\psi\psi}\psi^2\right) \tag{57}$$

is the generalization of a potential $V(\psi,\theta) = (\gamma/2)(\zeta-1)^2(1+c_{\theta+\psi}(\theta+\psi)^2)$ which could be implemented in a physical single-leg hopping robot by a passive leg spring and a passive torsional spring between the body and the leg. The generalized potential (57) would require passive springs attached to a "co-moving" inertial frame, preventing a physical implementation with a one-legged robot. However, we believe that this model reasonably approximates the moments due to the "outrigger" front and back legs, compressed against the horizontal ground surface, in the tripod stance phase of RHex.

## 4.2 Correspondence between RHex-like simulations and their fitted SLIP models

Simulations of a RHex-like hexapedal robot were run in SimSect [7] over a discretized range of clock parameters of RHex's open loop clock controller [1] that respect assumptions **R1**, **R2**, **R3** of Section 3.4.2: $t_c \in [0.235, 0.245], \varphi_s \in [0.84, 1.04], \varphi_0 \in [-0.16, 0.04], d_f \in [0.52, 0.6]$, where the duty factor $d_f$ is defined as $d_f = (t_c - t_s)/t_c$. Of the resulting 1815 SimSect simulations, 522 (= 29%) were stable according to the criteria of Appendix D.1. Then a 3 DOF SLIP model with the stance potential (57) and the leg angle trajectory (55) was fit to those stable cases following the fitting procedure outlined in Appendix D.2.

As is detailed below, the 3 DOF SLIP model approximates the 24 DOF SimSect steady state dynamics surprisingly well given the gulf in dimension. Specifically, the trajectory fitting errors are very small on average, the fixed points of the SimSect simulations and the fitted SLIP models are within the same order of magnitude, and the asymptotic behavior agrees in almost all cases.

However, while the fitted SLIP models provide good correspondence once a specific SimSect operating point has been selected, it is not the case that a priori specification of clock parameters yields a SLIP model whose fixed point locus and stability predicts that observed in the SimSect model. In this sense, the present SLIP model provides a descriptive but not prescriptive representation of the SimSect dynamics.

### 4.2.1 Correspondence of trajectories

The quality of the fit is assessed for each stable simulation by the two fitting error numbers $\Delta yz_{L_2}$ and $\Delta\theta_{L_2}$ as described in Appendix D.3. The average fitting error and standard deviation for both errors for the 522 stable SimSect simulations for the cartesian coordinates is small $\Delta yz_{L_2} = 3.82 \pm 0.42\%$ and of similar magnitude as the fitting errors for 2 DOF SLIP models observed in [34], whereas the average fitting error for the pitch coordinates $\Delta\theta_{L_2} = 93.65 \pm 25.76\%$ is considerably larger. As an illustration of the fitting results a sample SLIP fit is presented in Figure 7. The data trajectories of $y(t), \dot{y}(t), z(t), \dot{z}(t), \theta(t), \dot{\theta}(t), \zeta(t)$ are plotted together with the trajectories of their fitted SLIP models.

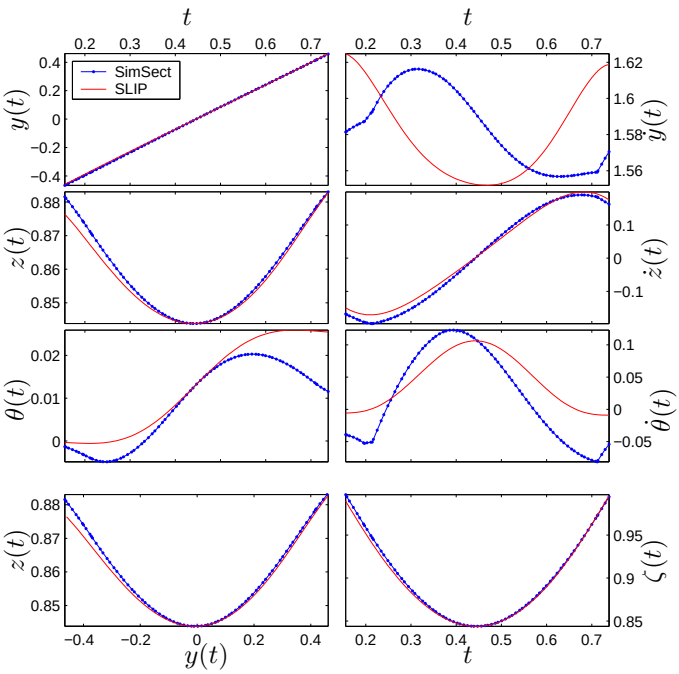


Figure 7: Trajectories of a stable SimSect simulation and the corresponding trajectories of the fitted SLIP model. The fitting errors are $\Delta yz_{L_2} = 3.56\%$ and $\Delta\theta_{L_2} = 51.46\%$.

The large $\Delta\theta_{L_2}$ fitting error is an indication that the proposed 3 DOF SLIP model is not a sufficiently accurate abstraction of SimSect's pitching dynamics. Another contributing factor to the size of $\Delta\theta_{L_2}$ is the fact that the magnitudes of both the $\theta(t)$ and $\dot{\theta}(t)$ trajectories are small, which makes the denominator of the fitting error $\Delta\theta_{L_2}$ (64) small. Another deviation of the dynamics of the fitted SLIP model from SimSect is apparent in the $\dot{y}(t)$ trajectories of Fig. 7 which is typical of all fitted SLIP models. Here, the

fitted SLIP trajectory is out of phase with the SimSect COM trajectory; nevertheless the fitting error $\Delta yz_{L_2}$ is small because of the large average value of the SimSect trajectory that enters (64). We believe that the acceleration in the forward direction during the leg compression phase seen in SimSect as opposed to a deceleration in the corresponding SLIP model is due to the non-conservative nature of the SimSect model, where energy is pumped into the system by the hip torques, and then lost to damping and friction.

#### 4.2.2 Correspondence of fixed points

Next we investigate whether the fixed point of the fitted SLIP model accurately predicts the fixed point of the corresponding SimSect run. In general, the fitted SLIP model with the initial condition obtained from its SimSect simulation as described in Appendix D.3 will not operate at a fixed point of its return map $R$. Hence a root-finding algorithm (Matlab's 'fsolve') is employed to determine the fixed point $\bar{x}_{\text{SLIP}}$ (if it exists) of the return map $R$ of the fitted SLIP model as well as the eigenvalues $\{\lambda_i\}_{i=1,...,4}$ of the Jacobian of the return map: $D_x R(\bar{x}_{\text{SLIP}})$. The fixed point $\bar{x}_{\text{SLIP}}$ is then compared to the "fixed point" $\bar{x}_{\text{Sim}}$ – the appropriate projection of the initial data point of the SimSect simulation stance data. Scatter plots of the components of the fixed points $\bar{x}_{\text{SLIP}}$ and $\bar{x}_{\text{Sim}}$ of all stable SimSect simulations are shown in Fig. 8. For perfect correspondence of the SimSect and SLIP dynamics, all fixed point components should lie on the identity lines. While the orders of magnitude of the components of the fixed points match, the components are in general not well correlated, except for $\bar{z}_{\text{SLIP}}$ and $\bar{z}_{\text{Sim}}$ if a constant offset is taken into account. The fixed points $\dot{\bar{z}}_{\text{Sim}}$ assume an almost constant value and the pitching components of $\bar{x}_{\text{SLIP}}$ are very close to zero and underestimate the magnitude of the pitching components of $\bar{x}_{\text{Sim}}$.

#### 4.2.3 Correspondence of stability at a fixed point

Given the numerically determined eigenvalues $\{\lambda_i\}_{i=1,...,4}$ of a fitted SLIP model at its fixed point $\bar{x}_{\text{SLIP}}$, its local asymptotic stability properties can be assessed. The magnitude of the determinant $|\Pi_{i=1}^4 \lambda_i|$ agrees to a high numerical precision with the appropriate expression in Table 1, predicting instability for $\varphi_0 > 0$ and allowing asymptotic stability for $\varphi_0 \geq 0$. However, SimSect simulations that are stable in the sense of Appendix D.1 are found with similar frequency of occurrence for $\varphi_0 > 0$ as well as for $\varphi_0 < 0$ for the range of clock parameters

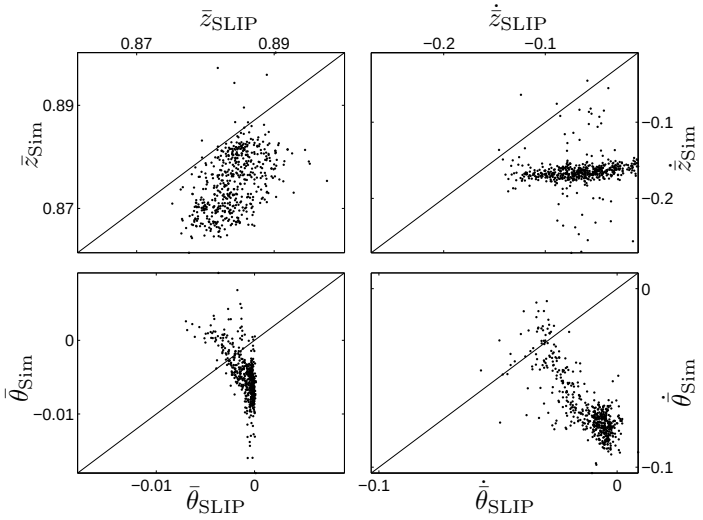


Figure 8: Scatter plots of components of the fixed points of stable SimSect simulations versus the corresponding fixed point components of the fitted SLIP models. For perfect correspondence, all points should lie on the identity line.

considered. On the other hand, if the magnitudes of the individual eigenvalues are only slightly larger than one, e.g. $|\lambda_i| < 1.05, i = 1, ..., 4$ as is the case for 92% of the 522 stable SimSect runs, then the instability might only be revealed after many iterations (see Fig. 3b for a "weakly" unstable trajectory of a 2 DOF SLIP model with $|\lambda_1| = |\lambda_2| \approx 1.007$). Hence the predicted instability of the fitted SLIP models for SimSect simulations with certain RHex clock parameters might not be discernible from stability given the criteria in Appendix D.1 due to the finite amount of simulation time for each simulation and and also due to the limitations of the SLIP-SimSect correspondence as discussed above.

## 5 Conclusions

In this paper we use the example of the SLIP locomotion model to show how factored analysis of the return map may be a useful new tool in the stability analysis of hybrid Hamiltonian systems. Specifically, we derive a necessary condition for the asymptotic stability of SLIP for an arbitrary leg angle trajectory as well as a sufficient condition for its instability. These conditions are formulated as an exact algebraic expression despite the non-integrability of the SLIP system. Hence leg recirculation strategies that violate the above condition can be discarded without recourse to cumbersome numerical simulations. We also use the closed form ex-

pressions to characterize the "cost" of sensing required for the imposition of "fast" transients in a variety of 2 DOF SLIP models that have appeared in the recent legged locomotion literature.

We finally apply this analysis to a particular 3 DOF SLIP model with pitching dynamics and a RHex-like leg recirculation strategy that satisfies the necessary condition for asymptotic stability in certain parameter regions. An accompanying numerical study shows that this model captures the salient aspects of the steady state dynamics of the robot RHex [1] (simulated in SimSect [7]) and accurately predicts the robot's stability properties.

This analysis provides for the first time a partial explanation for the surprisingly stable behavior observed empirically in the robot RHex. It also paves the way for a more principled investigation of detailed, biologically-motivated leg placement strategies in the LLS model [11] which captures many aspects of cockroach locomotion [12].

# 6 Acknowledgements

This work is supported in part by DARPA/ONR Grant N00014-98-1-0747 and DoE grant DE-FG02-95ER25238 (P. Holmes). Helpful discussions with R. Ghigliazza and R. Groff are gratefully acknowledged.

# A Time reversal symmetry of RHex-like leg angle trajectories

In this appendix we apply the condition in Lemma 2 to a particular family of leg recirculation schemes, thus proving the involutive nature of the corresponding time reversed flow map. In particular, we prove that the solution $t_{TD}(x_0)$ of the threshold equation (19) for $S_2 = G \circ F_2$ at $x_0 \in \mathcal{X}$ for a particular leg angle trajectory also solves the threshold equation at $S_2(x_0)$. We focus on the family of leg angle trajectories

$$\phi(t, x_0) = \alpha(t) + k\left(\arccos(z_0) + \theta_0\right) - \theta_0 - \dot\theta_0 t \quad (58)$$

where $\alpha(t)$ is an arbitrary analytic function of time. This family has the form of the RHex-like recirculation strategy (55). The threshold function $h_2(f_2^t(x_0), x_0, t)$ for a 3 DOF SLIP model reads

$$h_2(f_2^t(x_0), x_0, t) = z(t) - \cos(\phi(t, x_0)) \; . \quad (59)$$

Then using $G(x_0) = (z_0, -\theta_0, -\dot z_0, \dot\theta_0)^\top$ and

$$G \circ f_2^{t_{TD}}(x_0) = \begin{pmatrix} z_0 + \dot z_0 t_{TD} - \frac{t_{TD}^2}{2} \\ -\left(\theta_0 + \dot\theta_0 t_{TD}\right) \\ -(\dot z_0 - t_{TD}) \\ \dot\theta_0 \end{pmatrix} \quad (60)$$

the threshold function in Lemma 2 reads

$$\begin{aligned} h_2(G(x_0), G \circ f_2^{t_{TD}}(x_0), t_{TD}) &= \\ z_0 - \cos\Big(\alpha(t_{TD}) - \dot\theta_0 t_{TD} + k\arccos(z_0 + \dot z_0 t_{TD} - & \\ \frac{t_{TD}^2}{2}) - (\theta_0 + \dot\theta_0 t_{TD})(k-1)\Big) &= 0 \end{aligned}$$

For a solution of this equation with the leg recirculating only once during flight $\phi(t_{TD}, x_0) \in (\frac{3}{2}\pi, 2\pi)$. This must be taken into account when inverting the cosine:

$$\begin{aligned} & \arccos(z_0) = -\Big(\alpha(t_{TD}) - \dot\theta_0 t_{TD} + \\ & \qquad k\arccos(z_0 + \dot z_0 t_{TD} - \frac{t_{TD}^2}{2}) \\ & \qquad -(\theta_0 + \dot\theta_0 t_{TD})(k-1)\Big) + 2\pi \\ \Leftrightarrow \quad & \cos\left(k\arccos\left(z(t_{TD})\right)\right) - \cos\Big(\arccos(z_0) + \alpha(t_{TD}) \\ & -\dot\theta_0 t_{TD} - (\theta_0 + \dot\theta_0 t_{TD})(k-1)\Big) = 0 \\ \overset{k=1}{\Leftrightarrow} \quad & z(t_{TD}) - \cos\left(\phi(t_{TD}, x_0)\right) = 0 \end{aligned}$$

with $\phi(t, x_0)$ as in (58). For $k = 1$ this equation is equal to the original threshold equation (59) at $x_0$ and hence $t_{TD}(x_0)$ also solves the threshold equation for $S_2(x_0)$. Assuming that $t_{TD}(x_0)$ is also the minimal solution of the threshold equation at $S_2(x_0)$ for all $x_0 \in \mathcal{X}$, we can conclude that the time reversed flow map of the flight phase with a leg angle trajectory defined by (58) with $k = 1$ is an involution on $\mathcal{X}_{h_2} = \mathcal{X}$. According to Lemma 3 this means that $F_2 \circ G = R_2$ is also an involution. Then $|\det(D_x F_2(\bar x)| = 1$ at a fixed point $\bar x$.

# B Equivalence of apex and touchdown Poincaré sections

In section 3.3.1 it was noted that in [13, 15] one-dimensional Poincaré maps characterized by the apex event during flight phase were used to illustrate the asymptotic behavior of the constant leg touchdown, leg retraction, and "optimized selfstabilization" strategies for the 2 DOF SLIP model. On the other hand straightforward counting of dimensions

shows that the Poincaré section of a 2-dimensional SLIP model should be 2-dimensional: the dimensionless phase space $\widehat{\mathcal{X}} := \mathbb{R} \times \mathbb{R}^+ \times \mathbb{R}^2$ with elements $\widehat{x} = (y, z, \dot{y}, \dot{z})^\top$ is four-dimensional; conservation of energy $E(x) = E_0$ and the definition of the Poincaré section $\mathcal{P} := \{\widehat{x} \in \widehat{\mathcal{X}} : p(x) = 0, y < 0\}$ should reduce the dimension by two. For the Poincaré section denoting the touchdown event, $p(x) = \sqrt{y^2 + z^2} - 1$ whereas for the Poincaré section denoting the apex event, $p_A(x) = \dot{z}$. Using conservation of energy to eliminate $\dot{y}$, the reduced Poincaré sections can then be parametrized by $x = (z, \dot{z})^\top \in \mathcal{X}$ for the touchdown event and by $x_A = (y_A, z_A)^\top \in \mathcal{X}_A$ for the apex event. While for some singular leg placement strategies the reduction to a 1-dimensional Poincaré section at the touchdown event is obvious, e. g. for the constant leg touchdown angle strategy illustrated in Fig. 2 a), there is a priori no reason why the apex Poincaré section should only be parametrized by one variable.

In order to illustrate the equivalence of the discrete dynamical systems defined by the two different Poincaré sections, we give an explicit coordinate transformation between the coordinates of the two reduced Poincaré sections $\mathcal{X}$ and $\mathcal{X}_A$. Because of the reset of the $y$-coordinate at touchdown, this coordinate transformation $T_A$ relates the touchdown variables $x$ to the next apex variables $x_A$ and not to the previous apex variables. It has the form

$$\begin{array}{rcl} T_A : \mathcal{X} & \to & \mathcal{X}_A \\ \begin{pmatrix} z \\ \dot{z} \end{pmatrix} & \mapsto & \begin{pmatrix} y_A \\ z_A \end{pmatrix} \end{array}$$

where $y_A = \sqrt{1 - z_{LO}^2} + \left(\sqrt{2(E_0 - z) - \dot{z}^2}\right) \dot{z}_{LO}$ and $z_A = z_{LO} + \frac{\dot{z}_{LO}^2}{2}$ and $(z_{LO}, \dot{z}_{LO})^\top = G \circ R_1(x)$. In the notation of the controlled plant model (2), the control inputs – the apex to touchdown time $t_A = u_A$ and liftoff to touchdown time $t_{TD} = u$ – are related by

$$u_A(k) = u(k) - \dot{z}_{LO}(k) \ . \tag{61}$$

The difference between the two parametrizations arises in the structure of the controlled plant model maps $A$: the apex controlled plant model map $A_A$ decouples into two separate maps $A_z$ and $A_y$ that are independent of $y_A(k)$ because of the $y$ coordinate reset at touchdown:[14]

$$\begin{array}{rcl} (z_A(k+1), y_A(k+1))^\top & = & A((z_A(k), y_A(k))^\top, u_A(k)) \\ z_A(k+1) & = & A_z(z_A(k), u_A(k)) \\ y_A(k+1) & = & A_y(z_A(k), u_A(k)) \end{array}$$

[14] The formal expressions for $A_z$ and $A_y$ can easily be derived and are not given here.

Hence the only way that $y_A(k)$ can enter the apex return map $R_A$ is through feedback: $u_A(k) = t_A(k) = t_A(z_A(k), y_A(k))$. Omitting the variable $y_A(k)$ which denotes the horizontal distance between the toe pivot and the flight phase apex, a one-dimensional return map $z_A(k+1) = R_z(z_A(k)) = A_z(z_A(k), t_A(z_A(k)))$ results. For the 3 DOF SLIP model with pitching, the apex return map without $y_A(k)$ dependence reduces the dimension from 4 to 3.

This explains why the apex Poincaré section is a convenient parametrization if feedback is restricted to a subset of the Poincaré section coordinates. However, the touchdown Poincaré section seems to be a more natural choice for the description of physical systems, since the touchdown event is clearly easier to detect than the apex event, which requires velocity sensing.

# C Invariant tori near a fixed point of 2 DOF SLIP models

In this section we establish criteria for the neutral stability of fixed points of the return map $R$ of a legged locomotion model. The closed circles in Fig. 3d) suggest the existence of 1-dimensional $R$-invariant tori, on which $R$ acts quasi-periodically. This is reminiscent of area-preserving mappings which can possess KAM-tori (see [35] and references therein); however, as indicated in the determinant contour plot for the stance phase alone (Fig. 4), area is in general not preserved in a neighborhood of the fixed point of $R$, unless the leg placement policy is designed to exactly compensate for the determinant deviations of the stance phase. It is well known, on the other hand, that *reversible* dynamical systems can mimic the behavior of Hamiltonian systems in the sense that they can also exhibit KAM-tori ([38], for a review see [28]). We will show how, under certain assumptions, a theorem on reversible mappings [36] can be applied to establish the existence of $R$-invariant tori in a neighborhood of a fixed point.

## C.1 A theorem on invariant tori near a fixed point of reversible diffeomorphisms

Before stating the main theorem, several definitions and a lemma must be provided:

**Definition 4 (Involution of type $(p, q)$)** *Let $\bar{x} \in \mathbb{R}^N$ be a fixed point of the involution: $G(\bar{x}) = \bar{x}$. An involution is said to be of type $(p, q)$ with $p + q = N$ at $\bar{x}$ if the characteristic polynomial of the Jacobian*

*of $G$ at $\bar{x}$ reads $(-1)^N(\lambda+1)^p(\lambda-1)^q$. This is the general form of the characteristic polynomial at the fixed point, since any involution can be written in a neighborhood of its fixed point as a partial reflection [39].*

**Definition 5 (Reversible diffeomorphism)** *A diffeomorphism $R:\mathbb{R}^N\to\mathbb{R}^N$ is called reversible with respect to the involution $G$ if $G\circ R\circ G=R^{-1}$.*

**Lemma 4 (Composition of involutions)** *The composition $R=R_2\circ R_1$ of two involutions $R_1$ and $R_2$ is reversible with respect to each of them, i.e. $R_1\circ R\circ R_1\circ R=id=R_2\circ R\circ R_2\circ R$. Likewise, a diffeomorphism $R$ that is reversible with respect to the involution $R_2$ can be written as $R=R_2\circ R_1$ where $R_1$ is another involution [40].*

**Definition 6 (Symmetric fixed point of a reversible diffeomorphism)** *By Lemma 4 a diffeomorphism $R$ reversible with respect to the involution $R_2$ can be written as $R=R_2\circ R_1$. A fixed point $\bar{x}\in\mathbb{R}^N$ of $R$ is called symmetric if it is also a fixed point of $R_2$ [28].*

The reduced Poincaré map for SLIP models in this paper was factorized as $R=R_2\circ R_1$ (24). If $R_1$ and $R_2$ are involutions, then the following abridged version of Theorem 2.9 in [36, pages 147-152] can be applied:

**Theorem 4 (Invariant tori near a fixed point of a reversible diffeomorphism (M.B. Sevryuk, 1986))** *Let $R$ and $R_1$ be diffeomorphisms $R,R_1:\mathbb{R}^N\to\mathbb{R}^N$, analytic in a neighborhood of a common fixed point $\bar{x}\in\mathbb{R}^N$ and let $R$ be reversible with respect to $R_1$. Assume that the eigenvalues $\{\lambda_i,\bar{\lambda}_i\}_{i=1,\dots,N/2}$ of the Jacobian at the fixed point $D_xR(\bar{x})$ satisfy $\lambda_i\in\mathbb{S}^1\backslash\{-1,1\}$ and $\{\lambda_i\}_{i=1,\dots,N/2}$ are pairwise distinct. In addition assume that $R$ is nondegenerate, i. e. $\exists l\in\mathbb{N}$ such that $R\in\Psi_l^*$ (for a definition of $\Psi_l^*$ see [36]). Then the following holds:*

*a) In any neighborhood of $\bar{x}\in\mathbb{R}^N$ there exist $N/2$-dimensional tori invariant under $R$ and $R_1$. The action of $R$ on these tori is quasiperiodic, and the frequencies of this action are constant on those tori.*

*b) There exist neighborhoods $\mathcal{O}_\epsilon$ of $\bar{x}\in\mathbb{R}^N$ ($\lim_{\epsilon\to0}\operatorname{diam}(\mathcal{O}_\epsilon)=0$, $\mathcal{O}_{\epsilon_1}\subset\mathcal{O}_{\epsilon_2}$ if $\epsilon_1<\epsilon_2$) such that $\lim_{\epsilon\to0}\frac{\operatorname{mes}(\mathcal{G}_\epsilon)}{\operatorname{mes}(\mathcal{O}_\epsilon)}=1$ where $\mathcal{G}_\epsilon$ denotes the union of invariant tori in $\mathcal{O}_\epsilon$.*

*c) $R_1$ is an involution of type $(N/2,N/2)$.*

## C.2 Application to 2 DOF SLIP models

We will now argue that this theorem can be applied to the 2 DOF SLIP model with a RHex-like leg recirculation (49) with $k=1$ as suggested by Fig. 3d). The recirculation strategy (49) is clearly of the form (58), hence $R_2$ is an involution by the result of Appendix A. In Section3.1.1 it was shown that the partial stance return map $R_1$ is also an involution. Next we need to show that $R_i$ are analytic at the fixed point $\bar{x}\approx(0.8772,-0.0764)^\top$:

**Analyticity of the stance phase return map factor** In Section 2.4.2 the analyticity of the stance phase flow $\widehat{f}_1^{t(\widehat{x}_0)}$ was established. The corresponding threshold function $h_1$ (15) is analytic in $\widehat{x}(t)$ and $\widehat{x}_0$ if $\zeta\neq0$. By the implicit function theorem, $t_1(\widehat{x}_0)$ will be analytic as long as $\frac{d}{dt}\left(\zeta\left(\widehat{f}_1^t(\widehat{x}_0)\right)\right)|_{t=t_1(\widehat{x}_0)}\neq0$. At the fixed point $\bar{x}$, $\zeta=1\neq0$ and $\frac{d}{dt}\left(\zeta\left(\widehat{f}_1^t(\widehat{\bar{x}})\right)\right)|_{t=t_1(\widehat{\bar{x}})}=\bar{y}\dot{\bar{y}}+\bar{z}\dot{\bar{z}}\approx0.6829\neq0$. Hence $t_1(\widehat{\bar{x}})$ is analytic at $\widehat{\bar{x}}$. Since the composition of analytic functions is analytic, $\widehat{F}_1=\widehat{f}_1^{t_1(\widehat{\bar{x}})}(\widehat{\bar{x}})$ and $\widehat{S}_1$ are analytic at $\widehat{\bar{x}}$, and $R_1$ is also analytic at $\bar{x}$.

**Analyticity of the flight phase return map factor** In Section 2.4.2 the flight phase flow $f_2^{t(x)}$ was seen to be analytic. We focus on the leg angle trajectory (49). The corresponding threshold function $h_1$ (19) is analytic in $x_0$ and $t$ if $0<z_0<1$. By the implicit function theorem, $t_2(x_0)$ will be analytic as long as $\frac{d}{dt}\left(h_2(f_2^t(x_0),x_0,t)\right)|_{t=t_1(x_0)}\neq0$. At the fixed point $\bar{x}$, $0<\bar{z}\approx0.8772<1$ and $\frac{d}{dt}\left(h_2(f_2^t(G(\bar{x})),G(\bar{x}),t)\right)|_{t=t_2(G(\bar{x}))}=-\dot{\bar{z}}+\sin(\omega(-2\dot{\bar{z}})+\arccos(\bar{z})+\pi)\omega\approx-6.6551\neq0$. Hence $t_2(G(\bar{x}))$ is analytic at $G(\bar{x})$. Then the composition $F_2=f_2^{t_2(G(\bar{x}))}(G(\bar{x}))$ is analytic at $G(\bar{x})$, and $S_2$ and $R_2$ are analytic at $\bar{x}$.

If $R_i$ are analytic, then the composition $R$ is also analytic in $\bar{x}$ and by Lemma 4 in Appendix C.1 the return map $R$ is reversible with respect to both $R_2$ and $R_1$. The numerically determined eigenvalue of $R:\mathbb{R}^2\to\mathbb{R}^2$ at the fixed point $\bar{x}$ in Fig. 3d is $\lambda_1=-0.6956+\mathrm{i}0.7185\in\mathbb{S}^1\setminus\{-1,1\}$. The nondegeneracy condition cannot be verified rigorously due to the nonintegrable nature of the return map, but is assumed to hold since degenerate diffeomorphisms are exceptional in the sense that they constitute a variety of codimension one [41]. Then the theorem predicts one-dimensional tori around the fixed point which are invariant under

$R$ and $R_1$ and $R_2$, two of which are plotted in Fig. 3d. The quasiperiodicity of the action of $R$ is corroborated by the numerically determined trajectory of $R$. Theorem 4 also predicts that $R_1$ and $R_2$ are involutions of type $(1,1)$. For the flight phase partial return map $R_2$ this was established in Section 3.1.2. For the stance phase partial return map, the eigenvalues of the Jacobian of $R_1$ at the fixed point $\bar{x}$ were numerically determined to be $\approx 1, -1$.

# D SLIP fitting protocol

## D.1 SimSect simulations

1. A simulation must successfully complete 10 seconds of simulation time without crashing, i.e. by maintaining upright forward locomotion.

2. A simulation must be stable over the last 20 strides. A stride is a part of the trajectory between two isolated maxima of the $z$-component of the COM-trajectory. Stability is measured in terms of the maximal deviation of averaged linear and angular velocities at the minimum of the $z$-component of the COM-trajectory for the last 20 individual strides with respect to the respective averaged quantities over those strides.

3. The second to last stride of the simulation is selected and is required to exhibit a flight phase at the isolated maxima, i. e. none of SimSect's six legs touch the ground over a finite amount of time around these maxima. In addition, at the the minimum of the $z$-component of the COM-trajectory all three legs of the stance tripod are required to touch the ground, whereas all three legs of the flight tripod must be off the ground.

Once a SimSect simulation has passed all of the above conditions, it is called stable. Then a 3-DOF SLIP model is fit to the simulation data of the selected stride. The simulation data required for fitting is given by time series vectors $\tilde{\boldsymbol{y}}_{\text{Sim}}, \dot{\tilde{\boldsymbol{y}}}_{\text{Sim}}, \ddot{\tilde{\boldsymbol{y}}}_{\text{Sim}}, \tilde{\boldsymbol{z}}_{\text{Sim}}, \dot{\tilde{\boldsymbol{z}}}_{\text{Sim}}, \ddot{\tilde{\boldsymbol{z}}}_{\text{Sim}}, \tilde{\boldsymbol{\theta}}_{\text{Sim}}, \dot{\tilde{\boldsymbol{\theta}}}_{\text{Sim}}, \ddot{\tilde{\boldsymbol{\theta}}}_{\text{Sim}}$ which form the part of the stride trajectory where all three legs of the stance tripod of the SimSect model are on the ground whereas all three legs of the flight tripod are in the air ("stance phase").[15] Here the $y$-coordinate denotes the forward position of SimSect's COM, $z$ denotes the vertical position of the robot's COM, and $\theta$ denotes the pitch angle of the robot in the sagittal plane.

[15] The stance tripod of RHex and the SimSect model is formed by those three legs that are simultaneously in the slow phase of the RHex clock controller. The flight tripod is formed by the other three legs that are in the fast phase.

## D.2 Fitting procedure

The equations of motion for the SLIP's stance phase (13) and the equation for the total conserved energy in terms of dimensional variables can be written as

$$\begin{aligned} \tilde{m}\ddot{\tilde{y}} &= -\partial_{\tilde{y}} V(\tilde{y},\tilde{z},\tilde{\theta}) \\ \tilde{m}(\ddot{\tilde{z}}+\tilde{g}) &= -\partial_{\tilde{z}} V(\tilde{y},\tilde{z},\tilde{\theta}) \\ \tilde{I}\ddot{\tilde{\theta}} &= -\partial_{\tilde{\theta}} V(\tilde{y},\tilde{z},\tilde{\theta}) \\ \frac{\tilde{I}}{2}\dot{\tilde{\theta}}^2 &= \tilde{E}_0 - V(\tilde{y},\tilde{z},\tilde{\theta}) - \tilde{m}\tilde{g}\tilde{z} - \frac{\tilde{m}}{2}(\dot{\tilde{y}}^2+\dot{\tilde{z}}^2) \end{aligned} \tag{62}$$

with $V(\tilde{y},\tilde{z},\tilde{\theta}) = \frac{\tilde{\kappa}}{2}(\tilde{\zeta}-\tilde{\zeta}_0)^2(1+c_{\theta\theta}\tilde{\theta}^2+c_{\theta\psi}\tilde{\theta}\tilde{\psi}+c_{\psi\psi}\tilde{\psi}^2)$, $\tilde{\zeta} = \sqrt{(\tilde{y}+\Delta\tilde{y})^2+\tilde{z}^2}$, and $\tilde{\psi} = \arctan\frac{\tilde{y}+\Delta\tilde{y}}{\tilde{z}}$. We want to determine the a priori unknown parameters $c_f = (\tilde{\kappa}, \tilde{\zeta}_0, c_{\theta\theta}, c_{\theta\psi}, c_{\psi\psi}, \Delta\tilde{y}, \tilde{E}_0)$ by fitting the numerical data of a single stance phase of a SimSect simulation to the equations (62). The first five components of $c_f$ are parameters that determine the SLIP potential $V$. The sixth component $\Delta\tilde{y}$ resets the $y$-coordinate origin and hence determines the $y$-position of the foothold of the fitted virtual SLIP with respect to the stance data. The fitting parameters also include the total energy $\tilde{E}_0$, because in SimSect the total energy is not constant due to damping, frictional losses and hip motor torques.

In order to determine the fitting parameters $c_f$ a nonlinear fitting procedure (using Matlab's 'lsqcurvefit') is employed that computes

$$\min_{c_f} ||F_{fit}(c_f,\tilde{\boldsymbol{x}}) - \tilde{\boldsymbol{x}}_{fit}||_2^2 \tag{63}$$

where $\tilde{\boldsymbol{x}} = (\tilde{\boldsymbol{y}}_{\text{Sim}}, \tilde{\boldsymbol{z}}_{\text{Sim}}, \tilde{\boldsymbol{\theta}}_{\text{Sim}}, \dot{\tilde{\boldsymbol{y}}}^2_{\text{Sim}} + \dot{\tilde{\boldsymbol{z}}}^2_{\text{Sim}})$, $\tilde{\boldsymbol{x}}_{fit} = (\tilde{m}\ddot{\tilde{\boldsymbol{y}}}_{\text{Sim}}, \tilde{m}(\ddot{\tilde{\boldsymbol{z}}}_{\text{Sim}}+g), \tilde{I}\ddot{\tilde{\boldsymbol{\theta}}}_{\text{Sim}}, (\tilde{I}/2)\dot{\tilde{\boldsymbol{\theta}}}^2_{\text{Sim}})$, and $F_{fit}(c_f,\tilde{\boldsymbol{x}})$ is the expression obtained by inserting $\tilde{\boldsymbol{x}}$ into the right-hand side of the equations (62). Once a solution $c_f$ has been found, the quality of the fit must be quantified.

## D.3 Fitting error assessment

Instead of using the residual (63), which lacks an intuitive physical interpretation and does not represent an error measure in phase space, we compute fitting errors as in [4, 37]. The assessment of the quality of the fit proceeds in two steps. First, a SLIP simulation over the same period of time as the data trajectory is run with the fitted value of $c_f$. The initial conditions are taken to be the positions

and velocities of the data trajectory at the minimum of $\tilde{z}_{\text{Sim}}$.[16] Second, the resulting SLIP trajectories $\tilde{\boldsymbol{y}}_{\text{SLIP}}, \dot{\tilde{\boldsymbol{y}}}_{\text{SLIP}}, \tilde{z}_{\text{SLIP}}, \dot{\tilde{z}}_{\text{SLIP}}, \tilde{\boldsymbol{\theta}}_{\text{SLIP}}, \dot{\tilde{\boldsymbol{\theta}}}_{\text{SLIP}}$ are compared to the data trajectories by $L_2$ percent errors:

$$\Delta X_{L_2} = 100 \frac{||X_{\text{Sim}} - X_{\text{SLIP}}||_2}{||X_{\text{Sim}}||_2} \ , \qquad (64)$$

Here, $X \in \{\tilde{\boldsymbol{y}}, \dot{\tilde{\boldsymbol{y}}}, \tilde{z}, \dot{\tilde{z}}, \tilde{\boldsymbol{\theta}}, \dot{\tilde{\boldsymbol{\theta}}}\}$ and $||\cdot||_2$ is the standard 2-norm. In an effort to simplify the assessment of the fitting error, the quality of the fit is reported as two numbers — the average $L_2$ percent error of the cartesian coordinates $\Delta yz_{L_2} = (\Delta\tilde{\boldsymbol{y}}_{L_2} + \Delta\tilde{z}_{L_2} + \Delta\dot{\tilde{\boldsymbol{y}}}_{L_2} + \Delta\dot{\tilde{z}}_{L_2})/4$ and the average $L_2$ percent error of the pitch coordinates $\Delta\theta_{L_2} = (\Delta\tilde{\boldsymbol{\theta}}_{L_2} + \Delta\dot{\tilde{\boldsymbol{\theta}}}_{L_2})/2$.

# References


[1] U. Saranli, M. Buehler, and D.E. Koditschek. RHex: A simple and highly mobile hexapod robot. *The International Journal of Robotics Research*, 20(7):616–631, 2001.

[2] R. Altendorfer, N. Moore, H. Komsuoğlu, M. Buehler, H.B. Brown Jr., D. McMordie, U. Saranli, R. Full, and D.E. Koditschek. RHex: A biologically inspired hexapod runner. *Autonomous Robots*, 11:207–213, 2001.

[3] R. Blickhan and R. Full. Similarity in multilegged locomotion: Bouncing like a monopode. *J. Comp. Physiol.*, A(173):509–517, 1993.

[4] W.J. Schwind. *Spring Loaded Inverted Pendulum Running: A Plant Model*. PhD thesis, University of Michigan at Ann Arbor, 1998.

[5] R. Full and D.E. Koditschek. Templates and anchors: neuromechanical hypothesis of legged locomotion on land. *Journal of Experimental Biology*, 83:3325–3332, 1999.

[6] U. Saranli. *Dynamic Locomotion with a Hexapod Robot*. PhD thesis, University of Michigan at Ann Arbor, 2002.

[7] U. Saranli. Simsect hybrid dynamical simulation environment. Technical Report CSE-TR-437-00, University of Michigan, 2000.

[8] P.-C. Lin, H. Komsuoğlu, and D. E. Koditschek. A leg configuration sensory system for dynamical body state estimates in a hexapod robot. In *Proceedings of the International Conference on Robotics and Automation (ICRA) 2003, Taipei, Taiwan*, 2003.

[9] M.H. Raibert. *Legged Robots that Balance*. MIT Press, Cambridge, MA, 1986.

[10] T. Kubow and R. Full. The role of the mechanical system in control: a hypothesis of self-stabilization in hexapedal runners. *Philosophical Transactions of the Royal Society of London Series B - Biological Sciences*, 354(1385):849–861, 1999.

[11] J. Schmitt and P. Holmes. Mechanical models for insect locomotion: dynamics and stability in the horizontal plane I. Theory. *Biological Cybernetics*, 83:501–515, 2000.

[12] J. Schmitt, M. Garcia, R. Razo, P. Holmes, and R.J. Full. Dynamics and stability of legged locomotion in the horizontal plane: A test case using insects. *Biological Cybernetics*, 86 (5):343–353, 2002.

[13] A. Seyfarth, H. Geyer, M. Günther, and R. Blickhan. A movement criterion for running. *Journal of Biomechanics*, 35:649–655, 2002.

[14] R. M. Ghigliazza, R. Altendorfer, P. Holmes, and D. E. Koditschek. A simply stabilized running model. *SIAM Journal on Applied Dynamical Systems*, 2(2):187–218, 2003.

[15] A. Seyfarth, H. Geyer, and H. Herr. Swing-leg retraction: a simple control model for stable running. *Journal of Experimental Biology*, 206:2547–2555, 2003.

[16] R. Altendorfer, D. E. Koditschek, and P. Holmes. Towards a factored analysis of legged locomotion models. Technical Report CSE-TR-467-02, University of Michigan, 2002. to appear in *Proceedings of the International Conference on Robotics and Automation (ICRA) 2003, Taipei, Taiwan*.

[17] H.M. Herr and T.A. McMahon. A trotting horse model. *International Journal of Robotics Research*, 19 (6):566–581, 2000.

[18] H.M. Herr and T.A. McMahon. A galloping horse model. *International Journal of Robotics Research*, 20 (1):26–37, 2001.

[19] P. Holmes. Poincaré, celestial mechanics, dynamical systems theory and "chaos". *Phys. Rep.*, 193(3):137–163, 1990.


[16] Since total energy is not constant over a stance phase in SimSect, the $\dot{y}$-component of the initial conditions is scaled to the fitted total energy $\bar{E}_0$.

[20] W.J. Schwind and D.E. Koditschek. Approximating the stance map of a 2 DOF monoped runner. *J. Nonlin. Science*, 10(5):533–568, 2000.

[21] S.R. Bullimore, S.G. Usmar, and J.F. Burn. An approximate analytical solution to the planar spring-mass model of locomotion. manuscript, 2003.

[22] H. Geyer, A. Seyfarth, and R. Blickhan. Stability in spring-mass running – theory. manuscript, 2003.

[23] F. Scheck. *Mechanics: from Newton's laws to deterministic chaos*. Springer-Verlag, Berlin, 1999. Third edition.

[24] J. Guckenheimer and S. Johnson. Planar hybrid systems. In *Hybrid systems II: Lecture notes in computer science*, pages 202–225. Springer-Verlag, Berlin, 1995.

[25] A. Ruina. Nonholonomic stability aspects of piecewise holonomic systems. *Reports on mathematical physics*, 42 (1-2):91–100, 1998.

[26] M.J. Coleman and P. Holmes. Motions and stability of a piecewise holonomic system: the discrete Chaplygin sleigh. *Regular and chaotic dynamics*, 4(2):55–77, 1999.

[27] J.S.W. Lamb and J.A.G. Roberts. Time-reversal symmetry in dynamical systems: A survey. *Physica D*, 112:1–39, 1998.

[28] J.A.G. Roberts and G.R.W. Quispel. Chaos and time-reversal symmetry. Order and chaos in reversible dynamical systems. *Physics Reports*, 216:63–177, 1992.

[29] R. L. Devaney. Reversible diffeomorphisms and flows. *Trans. Am. Math. Soc.*, 218:89–113, 1976.

[30] W.J. Schwind and D.E. Koditschek. Characterization of monoped equilibrium gaits. In *Proc. IEEE Int. Conf. on Rob. and Aut.*, pages 1986–1992, Albuquerque, NM, 1997.

[31] R. Courant and D. Hilbert. *Methods of Mathematical Physics. Vol. 2, Partial Differential Equations*. Wiley-Interscience, 1989.

[32] H. Geyer, R. Blickhan, and A. Seyfarth. Natural dynamics of spring-like running: Emergence of selfstability. In *Proceedings of the Fifth International Conference on Climbing and Walking Robots (CLAWAR 2002)*, pages 87–92. Professional Engineering Publishing Limited, 2002.

[33] A. Seyfarth and H. Geyer. Natural control of spring-like running – optimized self-stabilization. In *Proceedings of the Fifth International Conference on Climbing and Walking Robots (CLAWAR 2002)*, pages 81–85. Professional Engineering Publishing Limited, 2002.

[34] R. Altendorfer, R. M. Ghigliazza, P. Holmes, and D. E. Koditschek. Exploiting passive stability for hierarchical control. In *Fifth International Conference on Climbing and Walking Robots (CLAWAR)*, pages 177–184, Paris, France, 2002.

[35] J. Moser. *Stable and random motions in dynamical systems*. Princeton University Press, 1973.

[36] M.B. Sevryuk. *Reversible Systems*. Number 1211 in Lecture notes in mathematics. Springer-Verlag, 1986.

[37] R. Altendorfer, U. Saranli, H. Komsuoğlu, D.E. Koditschek, H.B. Brown Jr., M. Buehler, N. Moore, D. McMordie, and R. Full. Evidence for spring loaded inverted pendulum running in a hexapod robot. In *Experimental Robotics VII*, pages 291–302. Springer Verlag, 2001.

[38] V.I. Arnol'd. Reversible Systems. In R.Z. Sagdeev, editor, *Nonlinear and Turbulent Processes in Physics*, volume 3, pages 1161–1174. Harwood Academic Publishers, 1984.

[39] S. Bochner. Compact groups of differentiable diffeomorphisms. *Ann. Math.*, 46(3):372–381, 1945.

[40] G.D. Birkhoff. The restricted problem of three bodies. *Rend. Circ. Mat. Palermo*, 39:265–334, 1915.

[41] M.B. Sevryuk. Personal communication.